METHODS FOR COST-EFFECTIVE SYNTHESIS OF HEPARAN SULFATE POLYSACCHARIDES

Susan Marian Woody

A thesis submitted to the faculty of the University of North Carolina at Chapel Hill in partial fulfillment of the requirements for the degree of Masters of Science in Pharmaceutical Sciences (Chemical Biology and Medicinal Chemistry).

Chapel Hill
2016

Approved By:

Jian Liu

Qisheng Zhang

Michael Jarstfer

ABSTRACT

Susan Marian Woody: Methods for cost-effective synthesis of heparan sulfate polysaccharides
(Under the direction of Jian Liu)

Heparin is a highly sulfated polysaccharide that is commercially available for anticoagulation. As an animal sourced product, heparin is heterogeneous and contains polysaccharides that differ in length and sulfation patterns. In 2007, heparin sourced from porcine intestines was contaminated with over-sulfated chondroitan sulfate. Taken in conjunction with other possible pharmacological activities, there have been efforts to synthesize distinct heparan sulfate polysaccharides in a cost-effective manner, including chemoenzymatic synthesis.

Some of the limitations associated with chemoenzymatic synthesis include expensive starting materials and incomplete synthesis leading to a product mixture. In an effort to overcome the first obstacle we developed two methods to efficiently synthesize the starting materials for heparan sulfate chemoenzymatic synthesis, including UDP-GlcNTFA and UDP-GlcA, from glucosamine and glucose respectively. To overcome the second obstacle, we explored possible inhibition by the chemoenzymatic co-factor PAPS. Both of these projects aim to advance the production of heparin and heparan sulfate polysaccharides.

To my parents, brother, and husband, who have guided me through all of my education; past, present and future.

To my dogs Arabella, Jordan, Itsy, and June, whose unending love and devotion always brought a smile to my face.

ACKNOWLEDGEMENTS

First of all, I would like to acknowledge my adviser Jian Liu, PhD whose encouragement and understanding was always welcome. He was more than willing to work with me through my education and training and has continued to help me pursue my goals. I am very thankful that I was able to work for him and appreciate all of the aid he has provided.

Secondly, I would like to thank all of my lab members, past and present. Their support when facing scientific problems and graduate school was great. Everyone was always willing to help out and made my time in the lab much more enjoyable. Special thanks to Ryan Bullis, PhD, Po-Hung Hsiesh, PhD, Yongmei Xu, PhD, Sherket Peterson, PhD, Vijay Pagadala, PhD, Truong Pham, Katelyn Arnold, and Tim O'Leary. You guys have been great to work with and I wish you all the best.

Lastly, I would like to thank my fellow graduate students that entered into the Chemical Biology and Medicinal Chemistry graduate program in 2010. You guys definitely made this a lot easier! Special thanks to Sarah Thacker, PhD, and Adam Friedman, PhD, who were available when needed for help and support.

TABLE OF CONTENTS

LIST OF TABLES

LIST OF FIGURES

LIST OF ABBREVIATIONS

2-OST	Uronosyl 2-O-Sulfotransferase
3-OST	Glucosaminyl 3-O-Sulfotransferase
6-OST	Glucosaminyl 6-O-Sulfotransferase
ADP	Adenosine Diphosphate
ATP	Adenosine Triphosphate
AST-IV	Arylsulfotransferase-IV
ATIII	Antithrombin III
C_5-Epi	C_5-Epimerase
cDNA	Complementary DNA
CS	Chondroitan Sulfate
dNTP	deoxy-Nucleotide Triphosphate(s)
DTT	Dithiothreitol
ESI-MS	Electrospray-Ionization Mass Spectrometry
EXT1	Exostosin Glycosyltransferase-1
EXT2	Exostosin Glycosyltransferase-2
FGF	Fibroblast Growth Factor
FGFR	Fibroblast Growth Factor Receptor
GAG	Glycosaminoglycans
Gal	Galactose
Gal-T1	Galactosyltransferase-I
Gal-T2	Galactosyltransferase-II

GalU	Glucose-1-Phosphate Uridyltransferase
Glc-1-P	Glucose-1-Phosphate
Glc-6-P	Glucose-6-Phosphate
GlcA	Glucuronic Acid
GlcA2S	2-O-sulfated Glucuronic Acid
GlcA-PNP	1-O-para-nitrophenyl-glucuronide
GlcATI	Glucuronyltransferase
GlcNAc	N-acetylglucosamine
GlcNAc6S	N-acetylated-6-O-Sulfated Glucosamine
GlcN	Glucosamine
GlcN-1-P	Glucosamine-1-Phosphate
GlcNS	N-sulfated Glucosamine
GlcNS6S	N-sulfated-6-O-Sulfated Glucosamine
GlcNTFA	N-acetyltrifluoroglucosamine
GlcNTFA-1-P	N-acetyltrifluoroglucosamine-1-phosphate
GlmU	N-acetylglucosamine-1-phosphate Uridyltransferase
HIT	Heparin Induced Thrombocytopenia
HPV	Human Papillomavirus
HS	Heparan Sulfate
HSPG	Heparan Sulfate Proteoglycans
HSV-1	Herpes Simplex Virus-1
hUDGH	Human-UDP-Glucose Dehydrogenase

IdoA	Iduronic Acid
IdoA2S	2-O-Sulfated Iduronic Acid
IPTG	Isopropyl β-D-1-thiogalactopyranoside
KfiA	N-acetylglucosaminyl Transferase
KH_2PO_4	Potassium Phosphate
LB	Luria Broth
LDH	Lactate Dehydrogenase
LMWH	Low Molecular Weight Heparin
MBP	Maltose-Binding Protein
NAD^+/NADH	Nicotinamide adenine dinucleotide
NAHK	N-acetylhexosamine 1-Kinase
NDST	N-deacetylase/N-sulfotransferase
NMR	Nuclear Magnetic Resonance
O.D.	Optical Density
PAP	3'-Phosphoadenosine-5'-Phosphate
PAPS	3'-Phosphoadenosine-5'-Phosphosulfate
PCR	Polymerase Chain Reaction
PF-4	Platelet-Factor 4
PGM	Phosphoglucomutase
pmHS2	Heparosan Synthase 2
PNP	Paranitrophenol
PNPS	Paranitrophenolsulfate

TEA	Triethylamine
UDP	Uridine Diphosphate
UDP-Glc	Uridine Diphosphate-Glucose
UDP-GlcA	Uridine Diphosphate-Glucuronic Acid
UDP-GlcNAc	Uridine Diphosphate-N-acetylglucosamine
UDP-GlcNTFA	Uridine Diphosphate-N-acetyltrifluoroglucosamine
UDP-Glc PPase	Uridine-5'-Diphosphoglucose Pyrophosphorylase
UFH	Unfractionated Heparin
USP	United States Pharmacopoeia
UTP	Uridine Triphosphate
VEGF	Vascular Endothelial Growth Factor
Xyl	Xylose

CHAPTER I

Introduction

Heparan sulfate and heparin

Heparan sulfate (HS) and heparin are anionic polysaccharides that belong to a group of molecules known as glycosaminoglycans (GAGs) (1). Other members of this same class of molecules include chondroitan sulfate (CS), keratan sulfate, and hyaluronic acid (2-3). Heparan sulfate, like the other glycosaminoglycans, is commonly found as a proteoglycan, meaning it is covalently bonded to a core protein. (1-6). Heparan sulfate proteoglycans (HSPGs) can be found in many cell types throughout the body (1, 2, 7). The core proteins most associated with heparan sulfate include syndecans, glypicans, agrin, perlecans, and collage-type XVIII (1, 8). These core proteins are associated with different parts of the cellular environment. Specifically, syndecans are tethered to the cell membrane via a transmembrane domain, and glypicans are attached to the membrane via a glycophosphatidylinositol linker. In comparison, agrin, perlecans, and collagen-type XVII are secreted into the extracellular environment (8).

Although closely related, heparan sulfate and heparin have differences related to their location and core proteins. In particular, heparin is only found in the cytoplasmic granules of mast cells, and is biosynthesized with the core protein serglycin (1, 4). After synthesis, heparin is cleaved by proteases for storage in mast cells (7). In comparison, heparan sulfate is more ubiquitously found throughout the body and is biosynthesized on various core proteins (1, 7).

Structure of heparan sulfate and heparin

In general, glycosaminoglycans contain a disaccharide unit of either galactosamine/ glucosamine with an uronic acid (3). In the case of heparan sulfate and heparin, the disaccharide unit consists of glucosamine (GlcN) and either glucuronic (GlcA) or iduronic acid (IdoA). These disaccharides are then typically modified during HS biosynthesis to produce the final product (7).

HS Biosynthesis: Initiation

The synthesis of HS in cells typically has three separate stages known as chain initiation, polymerization, and modification (1, 7, 9). In order to begin HS biosynthesis, it is necessary to add a tetrasaccharide linker to the core protein. The first sugar added is xylose (Xyl), which is added to the hydroxyl group of a specified serine residue on the core protein via xylosyltransferase. Upon the addition of xylose, two galactose (Gal) sugars are added by galactosyltransferase-I (Gal-T1) and galactosyltransferase-II (Gal-T2). The final step is the addition of a GlcA residue via glucuronyltransferase (GlcAT1) (9). The final tetrasaccharide linker has the following structure. GlcA-(1→3)-Gal-(1→3)-Gal-(1→4)-Xyl-1-O-Serine (7, 13).

HS Biosynthesis: Elongation

After formation of the tetrasaccharide linker, chain elongation begins. This is done by alternating the addition of GlcA and N-acetylglucosamine (GlcNAc) residues via (1→4) linkages (13). The enzymes responsible for elongation are Exostosin glycosyltransferase-1 (EXT1) and Exostosin glycosyltransferase-2 (EXT2) (9-11). It is thought that EXT2 acts more as a chaperone protein for EXT1 than as part of the elongation step itself (1, 9).

HS Biosynthesis: Modifications

The final step in the biosynthesis of HS is the modification of the sugar residues. The modification steps can be broken down into five separate alterations based on the enzyme performing the modification. These enzymes include N-deacetylase/N-sulfotransferase, (NDST), C_5-epimerase (C_5-epi), Uronosyl 2-O-Sulfotransferase (2-OST), Glucosaminyl 3-O-Sulfotransferase (3-OST), and Glucosaminyl 6-O-sulfotransferase (6-OST). The final modifications are not homogenous along the entire HS chain, and give rise to differing HS structures that are thought to play a key role in the multiple biological roles of HS (12).

N-Deacetylation/N-Sulfation

NDST modifies the GlcNAc residues of the elongating HS chain to create N-sulfated glucosamine (GlcNS) sugars using the sulfur donor 3'-phosphoadenosine-5'-phosphosulfate (PAPS) (9). In total, there are four isoforms of NDST (2, 13). The isoform most associated with the production of heparin is NDST-2, as it is the isoform most commonly found in mast cells (13). It is also thought that certain forms of NDST may be capable of deacetylation without subsequent sulfation, leading to deacetylated glucosamine (GlcN) residues in the final product (9).

The modification done by NDST plays a key role in the final structure of HS. More specifically, regions where GlcNS residues are present tend to refer to highly sulfated domains. In comparison, un-sulfated or under-sulfated domains of HS are denoted by the presence of GlcNAc residues (1).

Epimerization

After N-sulfation, epimerization and O-sulfation occur to the growing HS chain. The C_5-epimerase acts on GlcA residues based on the presence of GlcNS at the non-reducing end of the

chain to convert GlcA to IdoA (2). In comparison to NDST, there is only one known isoform for C_5-epimerase (13).

O-Sulfation

Similar to C_5-epi, there is also only one known isoform of 2-OST. This sulfotransferase is able to add a sulfate group at the C_2 position of IdoA creating 2-O-sulfo iduronic acid (IdoA2S), or less frequently to the C_2 position of GlcA creating 2-O-sulfo glucuronic acid (GlcA2S) (9, 13). As with C_5-epimerase the presences of GlcNS greatly aids in the addition of 2-O-sulfation (3).

The last two modifications are 6-O sulfation and 3-O sulfation of the glucosamine residues in the growing HS chain (2). 6-OST has three different isoforms and the most common modification is to the C_6 position of a GlcNS residue, creating GlcNS6S. While this is the predominant pattern, occasionally GlcNAc can be sulfated at the C_6 position to create GlcNAc6S. As for 3-O-sulfation, it is the least common modification. 3-OST has seven known isoforms and will typically add a sulfate to the C_3-position of either a GlcNS or GlcNS6S residue (2, 7). However, there have also been reports of 3-O-sulfation on GlcN residues (13). Overall, it is thought that the 3-O sulfation is an important modification for pharmaceutical and biological actions of final HS molecules (2).

Final Composition

The final HS chain contains one of two disaccharide units. One possible unit is between glucosamine and glucuronic acid, and the other possible unit is between glucosamine and iduronic acid. The sites of possible modification are highlighted in red below (Figure 1). It is important to remember that a lot of the sulfation patterns will depend on the specificity of the enzyme isoform that is present and/or the surrounding HS structure (13).

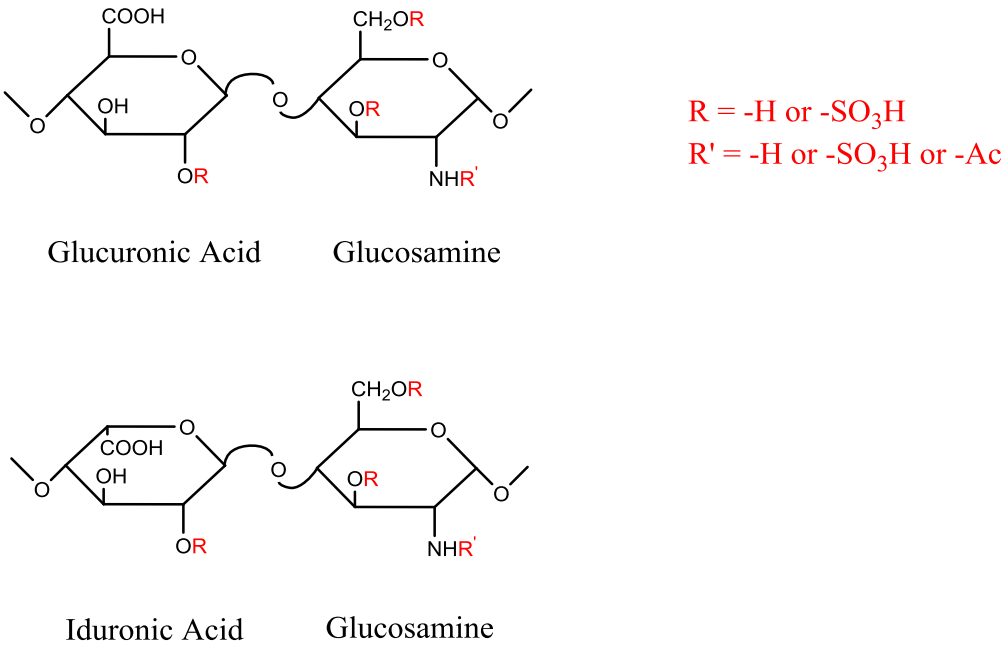

Figure 1: Disaccharide units of HS polysaccharides. The possible modifications for HS polysaccharides are shown. Figure adapted from (12).

Other modifications

Upon complete biosynthesis, the HS structure can still be modified (7, 14). The first alteration involves two enzymes known as endosulfotases that can remove 6-O-sulfations, usually in highly sulfated regions of HS (9). Another modification involves the enzyme heparanase that can break HS into smaller chains, often 10-20 sugars in length (14).

Structural Distinctions between HS and Heparin

Heparin is not only distinct from HS in its core protein and location in the body, but in its final modification pattern as well. Specifically, heparin has what are known as “highly sulfated” domains, marked by a large number of sulfations on the polysaccharide backbone. In particular, there are 2.5-3 sulfo groups per disaccharide unit in heparin, compared to 0.5-1.5 sulfo groups per disaccharide unit in HS (1). Moreover, about 80% of the uronic acids in heparin are IdoA, compared to about 20% in HS (2). Due to the high level of sulfation, heparin is regarded as the most anionic biological macromolecule known (4).

Activity of Heparan Sulfate in the body

The variable HS structures allow for numerous protein interactions that give rise to many different biological and pharmaceutical functions as described below. Moreover, some of these interactions are thought to be dependent on specific HS sequences, while some may depend on less specific binding interactions (1, 15).

Viral Infection

HS proteoglycans and their structures have been implicated as playing a role in viral infections, including human papillomavirus (HPV) that can have long term health effects (15-16). For instance, a virus binding to a cell's exposed HS or HS proteoglycans can facilitate viral entry, along with other functions (1, 16-17).

One classic example of HS viral interaction is with Herpes Simplex Virus-1 (HSV-1), a virus that is currently causing an increase in the number of genital warts cases in the U.S. (18). Research has shown that an HS octasaccharide region containing a 3-O-sulfation interacts with the HSV-1 glycoprotein D. This interaction plays a critical role in the fusion of the virus with the host cell leading to further HSV-1 proliferation (1-2, 17).

Other viral infections where HS plays a mediating role include human papillomavirus as mentioned previously. In this situation, the viral particle must bind to a syndecan or glypican proteoglycan in order to enter a cell. HS has also been implicated as an important mediator of attachment for non-viral infections such as Chlamydia (1). Due to the nature of these interactions, the discovery of specific HS structures that are involved in viral binding with HS or HSPGs may offer information on novel methods for preventing viral entry and proliferation.

Cell Proliferation and Differentiation

Besides interacting with exogenous proteins, HS also interacts with several endogenous molecules including numerous growth factors and receptors. In particular, HS has been reported to interact with fibroblast growth factors (FGFs), their corresponding receptors (FGFRs), vascular endothelial growth factor (VEGF), and other molecules (15).

One of the best studied interactions is between HS and FGF-2. FGF-2 is a growth factor that can bind FGFRs and is associated with cell proliferation (7). In order to bind FGF-2, a small HS oligosaccharide consisting of 4-6 sugars with an IdoA2S modification must be present. If the oligosaccharide is longer (10 sugars) and includes a 6-O-sulfation then HS binding to the corresponding FGFR also becomes possible, and potentiates signaling in the cell (9, 15). There is evidence of HS inhibiting other growth factors as well, and it is believed that this is due to the complex structural design of HS that is mediated by specific cells (19).

HS has also been implicated in binding with hepatocyte growth factor, platelet-derived growth factor, and others (19). Therefore, determination of any crucial HS structural components that potentiate growth would be helpful in understanding how cells mediate growth and binding.

Tumor Development

The relationship between HS and cancer is complex as it can both inhibit and accelerate cancer growth (2, 20). As mentioned with cell proliferation, HS is involved in binding growth factors and potentiating signaling. As such, HS is thought to be important for initial tumor development and related angiogenesis that sustains growth (21).

Furthermore, with the over expression of heparanase, initial tumor growth due to HS can become a malignant cycle. More specifically, the over-expression of heparanase has been shown to increase the solubility of VEGF and FGF-2 thereby increasing the possibility of harmful

signaling. Heparanase over-expression is also associated with an up-regulation of HSPGs that can lead to an increase in destructive signaling. Finally, heparanase was recently shown to increase exosome release from malignant cells thereby making the neighboring environment more conducive for cancer (14).

While the role of HS is unclear, HSPGs are associated with positive and negative outcomes. In fact, while the HSPG syndecan-1 is thought to promote tumor progression, the HSPG syndecan-2 can act to prevent or reduce metastasis through interactions with integrins (22). These numerous effects suggest that more information is needed about the structural portions of HS and HSPGs that interact with proteins associated with cancer.

Inflammation

Inflammation, while usually associated with injury, can also be related to disease states in humans (23). The role of HS in inflammation comes from its ability to guide leukocytes to the site of damage or injury (9, 21, 23). Specifically, HS is critical for binding the leukocyte's L-selectin protein, and slowing down the leukocyte so that it can enter the site of injury (24).

According to work published by Wang et al., under sulfation of HS via an endothelium NDST-Isoform 1 knockout led to fewer neutrophils entering the site of injury because L-selectin was unable to bind and slow down neutrophils (21, 24). Moreover, the authors showed that HS helps to present chemokines that cause a firmer bond between leukocytes and endothelial cells at the site of injury (24). As stated previously, this information suggests that understanding the role between the structure of HS and binding to endogenous molecules is necessary for a full understanding of inflammatory responses.

Anticoagulation

While the *in-vivo* biological activity of heparin is not associated with anticoagulation, it is still the reason why heparin became such a widely studied molecule (1, 9). In order to understand its mechanism of action however, it is critical to understand the coagulation cascade that potentiates the formation of fibrin, and therefore a clot (9, 25).

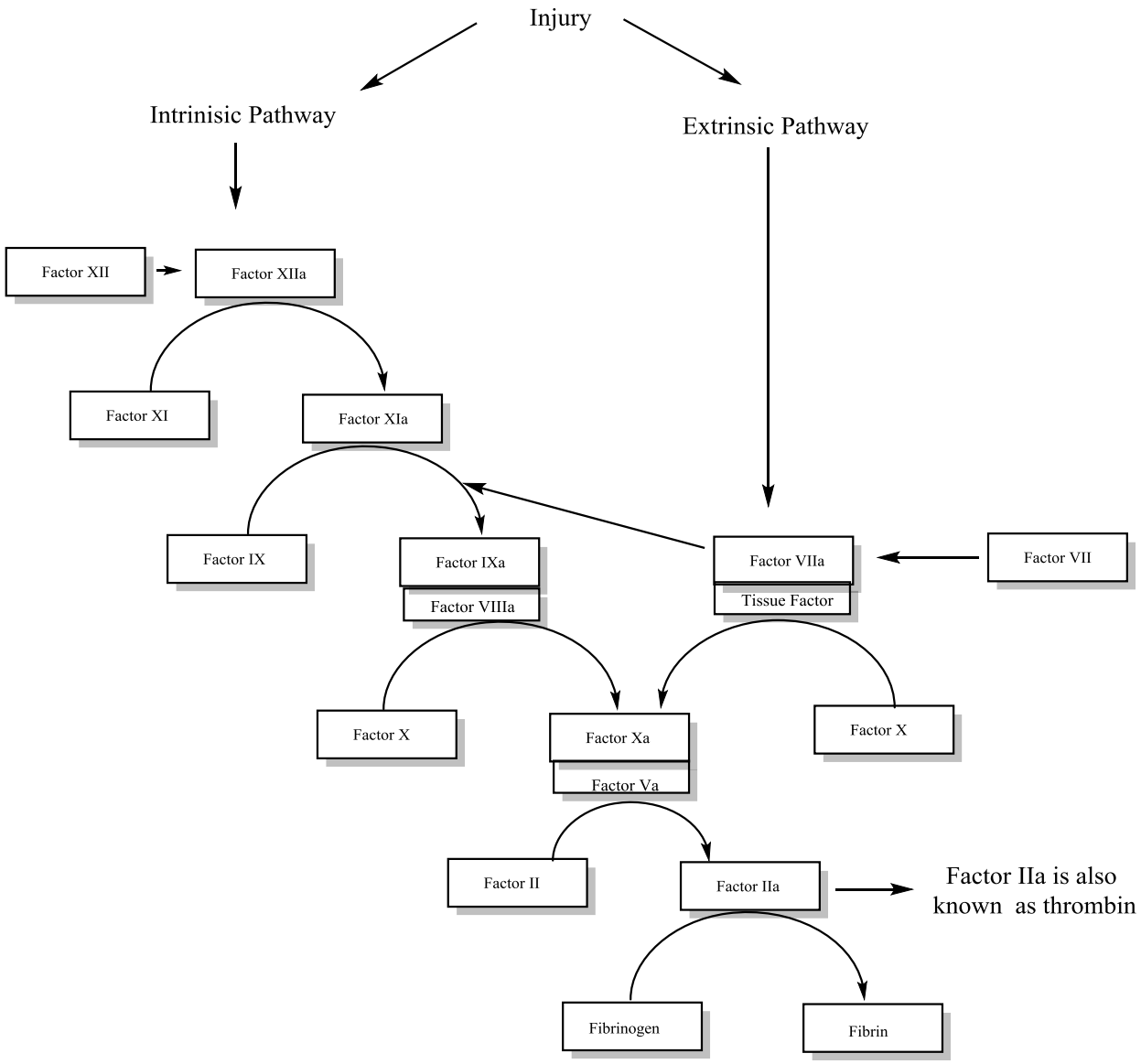

Figure 2: The Coagulation Cascade. There are two portions of the coagulation cascade called the intrinsic and extrinsic pathway. Both pathways lead to the activation of Xa (a serine protease) that cleaves thrombinoplastin (Factor II) to thrombin (Factor IIa). Thrombin in turn creates fibrin from fibrinogen, a critical portion of clotting. Heparin's mechanism of action affects Factors Xa and IIa. Figure adapted from (9 and 25).

Heparin is able to slow down the conversion of fibrinogen to fibrin by potentiating antithrombin III (ATIII) binding and subsequent inactivation of several pro-coagulants, most notably thrombin and factor Xa (9, 25). The binding between heparin and antithrombin III has been shown to require a specific pentasaccharide sequence as shown below (9) (Figure 3):

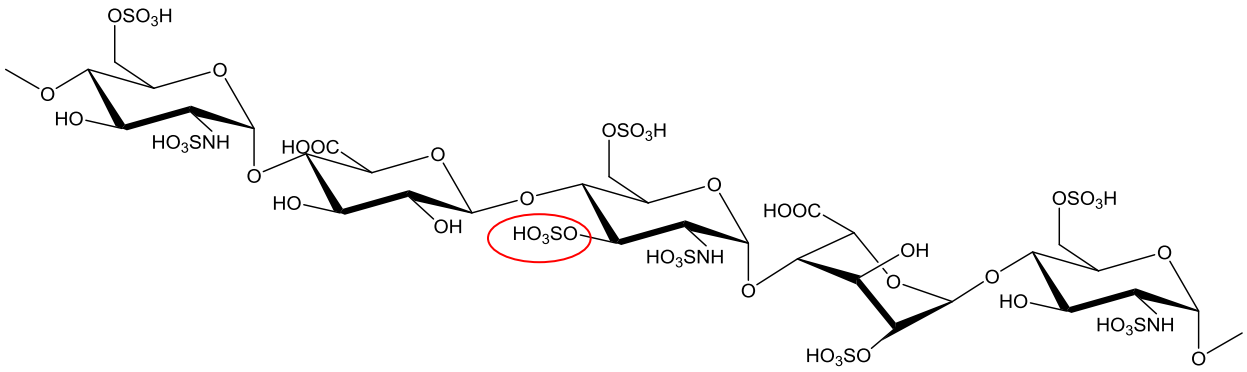

Figure 3: The ATIII binding domain of heparin. The pentasaccharide sequence responsible for ATIII binding. Note that the 3-O-sulfation circled in red is key for binding. Figure adapted from (13).

Heparin is able to bind antithrombin III with this minimum pentasaccharide sequence and intensify its activity against proteins of the coagulation cascade. However, it is critical to realize that in order for heparin to potentiate binding between antithrombin III and thrombin, a minimum chain length of 16-18 saccharides is necessary. On the other hand, in order for antithrombin III and factor Xa to bind, only the pentasaccharide sequence is necessary. This is important as there are many heparin and heparin-like products on the market with varying polysaccharide chain lengths that cannot potentiate a bond between antithrombin III and thrombin, possibly reducing adverse reactions associated with longer heparin molecules (1, 9).

One such adverse reaction is the development of an antigenic complex between heparin and Platelet Factor-4 (PF-4), leading to the formation of antibodies. The development of these antibodies can lead to platelet and monocyte activation, causing a pro-thrombotic state and life-threatening situation known as heparin induced thrombocytopenia (HIT). However, even though antibodies can form, they do not always lead to a pro-thrombotic state (26). Specifically,

variability exists in the rate of HIT based upon the size of the heparin or heparin-like molecule used (27). Taking this information into account suggests that there are unknown structure/ function relationships between heparin and natural biological compounds in the body that need to be explored.

Heparin production and modification for use as a pharmaceutical

In the United States, there are currently three different classes of heparin-like drugs on the market for use as an anticoagulant. The first drug class is isolated as an unmodified polysaccharide from pig intestinal mucosa, and is commonly referred to as Unfractionated Heparin (UFH). The second class is known as low-molecular weight heparin (LMWH) and is isolated in a similar manner to UFH, but is then either chemically or enzymatically degraded to form shorter polysaccharides before being used as an anticoagulant. The final product is called fondaparinux, a chemically synthesized pentasaccharide that is a replica of the pentamer required for antithrombin III binding. These different products lead to different pharmacological properties in humans including half-life, clearance and reversibility. A more detailed comparison can be seen in Table 1(9, 28-32).

Heparin-Type	**UFH**	**LMWH**	**Fondaparinux**
Mechanism of Action	Xa and IIa	Xa and IIa	Xa
Half-Life	~1 hour	~4 hours	~17 hours
Occurrence of HIT	<5%	<1%	<1%
Renal adjustment?	No	Yes	Yes
Protamine reversibility?	Complete	Partial	None
Source	Animal	Animal + De-polymerization	Synthetic

Table 1: **Comparison of UFH, LMWH, and fondaparinux.** Comparison of the three heparin products on the market including mechanism of action, half life, occurrence of HIT, renal considerations, potential for reversibility and product source. Table taken and adapted from (32).

Unfractionated Heparin

Heparin was initially isolated in the early twentieth century by a medical student, who found the product to have anticoagulant properties. Later, it was found that the initial product was contaminated with phospholipids, but as methods for refinement improved, heparin was also found to promote anticoagulation (9).

It is thought that besides anticoagulant activity, UFH has some anti-inflammatory and anti-cancer pharmacological effects, but anticoagulation remains heparin's primary use (1). Currently in the United States, heparin is isolated from porcine mucosa, although historically it has come from multiple sources including bovine lung. One of the issues with animal isolation is that heparin is a heterogeneous mixture of polysaccharides with an average molecular weight of 14,000 (9, 33). Therefore, in order to accurately dose heparin, it must be compared to a standard created by the United States Pharmacopoeia (USP), and is dosed in units for various diseases states (9). Method(s) to create a uniform mixture of heparin could help to avoid such requirements, but are currently unavailable.

The advantages offered with UFH compared to LMWH and fondaparinux include its short half-life and hepatic elimination. The short half life can be ideal for situations such as surgery, and clearance via the liver avoids renal dosing adjustments (28). However, UFH has the highest rate of heparin-induced thrombocytopenia among all of the heparin-like molecules (26). The reason for the increased rate of HIT remains unclear as there is no homogenous mixture in heparin, and the structures most likely to lead to HIT remain unknown. Therefore the creation of large quantities of homogenous heparin polysaccharides could be helpful in understanding HIT pathogenesis.

Low molecular weight heparin

In the 1970s, Dr. Edward Johnson performed a study in which he compared low molecular weight heparin obtained via gel filtration to high molecular weight heparin. He noted that the low molecular weight heparin had a longer inhibition of factor Xa than high molecular weight heparin or UFH. This prompted more investigation into LMWHs as a pharmaceutical alternative to heparin (9).

The first studies of low molecular weight heparin in humans were promising and therefore several manufacturers began to mass produce the product. In the end, three methods of de-polymerizing heparin were developed including nitrous acid degradation, enzymatic cleavage and β-elimination (9). Due to the smaller size, low molecular weight heparins are generally considered factor Xa inhibitors, with some factor IIa inhibition, but the factor IIa inhibition is not as strong as with heparin (34).

The LMWHs currently on the market in the United States include Enoxaparin, Dalteparin and Tinzaparin. In comparison to heparin, the molecular weight of these products ranges from 4,500-6,500 (34). Note that the different methods of preparation due lead to some pharmacological differences between the LMWHs, but the clinical relevance of these differences is still debated (28).

One advantage of these products includes their longer half life in the setting of preventative disease and the outpatient setting. Moreover, in comparison to UFH, LMWHs have a reduced risk of HIT. However, there are some drawbacks, including a lack of full reversibility. Moreover, while LMWHs can be used in renal impairment, the dose must be adjusted and the adjustment can depend on the product in use. (28).

Chemical Synthesis and Fondaparinux

The newest heparin-like molecule is fondaparinux, which was approved in 2002 (35). This molecule is the chemically synthesized version of the pentasaccharide domain in heparin necessary for ATIII binding. As such, it is generally considered a factor Xa inhibitor only (9).

One of the largest advantage's of the chemically synthesized fondaparinux include its more defined structure with a specific molecular weight of 1508.3 (33, 35-36). Moreover, the occurrence of HIT with fondaparinux is low, and it has even been used as a treatment for HIT (26). Its longer half life can also be an advantage in some situations, offering once a day dosing. However, in comparison to the heparins, it is not reversible, and cannot be used in extreme renal impairment (31, 37).

Even with these considerations, one of the biggest flaws of fondaparinux is the difficulty of its synthesis leading to a higher price than the heparin natural products (35). In particular, it takes about 50 synthetic steps with a 0.1% yield to produce fondaparinux (38). As such, increasing the cost-effective synthesis of this product could yield a larger earning margin for manufacturers. One possible method for this is to avoid chemical synthesis alone and focus on chemoenzymatic synthesis.

Safety Concerns

Currently, heparin is isolated from porcine intestines and as such is a heterogeneous natural product with varying polysaccharide lengths and different sulfation patterns (33). This heterogeneity creates an inherent concern in the use of heparin, as there are portions with unknown structure and/or functions.

A disparaging example of this concern occurred in 2007 when heparin supplies were contaminated with over-sulfated chondroitan sulfate supplied by Baxter. Initially the reactions

were considered “allergic reactions”, but as time went on the contamination outbreak led to over 100 deaths in America, plus international contamination. (39).

Over the course of 2008, the culprit was found to be over-sulfated chondroitan sulfate. In due process, the contamination led to the addition of three identity tests for heparin as mandated by USP (9). However, these changes only occurred after the adverse effects, and there is still a concern that the manufacturing process is providing patients a product of unknown composition. Therefore it has become important to develop cost effective methods for the synthesis of heparin (39).

Chemoenzymatic synthesis of heparin as an alternative approach

Chemoenzymatic synthesis of heparan sulfate and heparin offers an alternative to the intensive and low yield chemical synthesis of HS polysaccharides, especially with the successful expression of recombinant HS biosynthetic enzymes (1, 40). One of the first barriers in establishing chemoenzymatic synthesis is the expression of recombinant enzymes involved in the biological synthetic pathway. In the case of HS polysaccharide synthesis, expression of the required enzymes has been possible, except for EXT-1, EXT-2 and NDST (40).

EXT-1 and EXT-2 have not been successfully expressed. Instead two bacterial enzymes have been cloned and successfully used in chemoenzymatic synthesis to form the HS backbone (40). The first is heparosan synthase 2 (pmHS2) from *Pasteurella multicida*, that is able to add a glucuronic acid residue to the growing HS chain using the sugar donor uridine-diphosphate glucuronic acid (UDP-GlcA) (38, 40). The second enzyme is N-acetylglucosaminyl transferase (KfiA) from *Escherichia Coli* strain K5 that is able to add glucosamine residues (38, 40). As discussed previously, the glucosamine residue is crucial as it undergoes N-sulfation, a

modification that can facilitate other actions such as C_5 epimerization and 2-O-sulfation (38, 40). However, adding the N-sulfation has been problematic due to the lack of NDST expression.

NDST has proven to be a difficult enzyme to replicate because the N-sulfation domain of NDST is the only portion adequately expressed (40). Therefore, it has been difficult to add an N-sulfation group to glucosamine residues as it was not possible to deacetylate a naturally occurring N-acetyl glucosamine residue. Therefore, an unnatural sugar donor, called uridine-diphosphate N-acetyltrifluoroglucosamine (UDP-GlcNTFA) has been substituted where the presence of GlcNS is required. This donor adds N-acetyltrifluoroglucosamine (GlcNTFA), which can be de-trifluoroacetylated under basic conditions. Following this, N-sulfation can be added to the GlcN residue via the use of the N-sulfation domain of NDST.

The other enzymes required for chemoenzymatic synthesis, including C_5-epimerase, 2-OST, 3-OST (isoforms 1, 3 and 5) and 6-OST (isoforms 1 and 3), have all been expressed as recombinant enzymes with effective activity for synthesis of diverse HS polysaccharides (40).

For current HS polysaccharide biosynthesis, the starting material, 1-O-para-nitrophenyl-glucuronide (GlcA-PNP), is elongated using pmHS2 and KfiA. The sugar donors are UDP-GlcA for pmHS2 and UDP-GlcNTFA or uridine-diphosphate N-acetylglucosamine (UDP-GlcNAc) for KfiA depending on the desired final HS product (38, 41). After elongation reaches a pentasaccharide, the next step is N-sulfation of the GlcNTFA residues. First, the trifluoroacetyl group is removed under basic conditions before N-sulfation occurs using the NS domain of NDST and the co-factor PAPS. With the completion of N-sulfation, the HS polysaccharide is epimerized and 2-O-sulfated. The final steps include the addition of 6-O-sulfo and 3-O-sulfo groups. Note that these steps do have to be done in a specific order depending on the specific HS polysaccharide that is desired (38, 41).

As mentioned previously, the HS polysaccharide biosynthesis enzymes have preferred substrates so it is important to ensure that the correct substrates and modifications are added in the correct order. Using this method, low molecular weight heparin polysaccharides have been successfully synthesized on the milligram scale. One particular low molecular weight heparin, with strong anticoagulant action and reversibility comparable to UFH took only 22 steps and had about 10% yield, as compared to the 50 steps and 0.1% yield of fondaparinux (38, 40-41). This is a great example of the possibilities of HS synthesis using chemoenzymatic techniques.

Structural identification of chemoenzymatic HS polysaccharides

One of the problems with the 2007 contamination of heparin was that the presence of over-sulfated chondroitan sulfate was unknown until after production and distribution. Furthermore, in the current production environment, heparin identification testing does not identify the specific structure of every heparin molecule. Instead, heparin is standardized to provide a certain amount of anticoagulation, with additional identity tests for possible contaminants (9).

The best way to avoid another incident like 2007 is with a synthetic method that produces one heparin product. However, this concern cannot be completely eliminated from chemoenzymatic synthesis, as the reaction does not always proceed to completion. Even with purification, it can be difficult to determine the exact structure of an HS polysaccharide that was synthesized, especially as size increases. Furthermore, with increasing size comes difficulty with proton nuclear magnetic resonance (NMR) and mass spectrometry due to complexity. One way to overcome this obstacle is to introduce isotopically labeled ^{13}C into the HS polysaccharide to verify the final product from a specific synthetic method. However, the introduction of a ^{13}C would require the development of an isotopically labeled sugar donor at high levels.

STATEMENT OF PROBLEM

Chemoenzymatic synthesis offers options for the design of HS polysaccharides with specific functions. However, there are still several barriers to production, including how to effectively scale up the synthesis of HS polysaccharides in a cost-effective manner. One such barrier is the cost of the two starting sugar-nucleotides, UDP-GlcNTFA and UDP-GlcA. While our lab is capable of producing UDP-GlcNTFA effectively, the starting material, Glucosamine-1-Phosphate (GlcN-1-P) is about 200 dollars for 5mg versus about 40 dollars for 25 grams of glucosamine (42, 43). The other starting material, UDP-GlcA is about 1600 dollars for 1g versus about 20 dollars for 100 grams of glucose (44, 45).

Based on this information and using previous reports of sugar-nucleotide chemoenzymatic synthesis on a large scale, the first objective was to develop and implement two synthetic methods to reduce the cost of UDP-GlcNTFA and UDP-GlcA. The first method involved chemoenzymatic synthesis of UDP-GlcNTFA from glucosamine. Following completion of this work, the next step was to enzymatically synthesize UDP-GlcA from glucose. Each method would reduce the cost of starting materials and the resulting production cost of HS polysaccharides.

Another barrier to chemoenzymatic synthesis is how to maximize yield and avoid enzymatic inhibition. As mentioned previously, one of the cofactors involved in the reaction is the sulfo-group donor PAPS. There has been a concern that the by-product, 3'-phosphoadenosine-5'-phosphate (PAP), may inhibit some biosynthetic enzymes, limiting production (2). Therefore the final goal was to attempt to minimize any PAP inhibition.

CHAPTER II

Materials and Methods

Chemoenzymatic synthesis of UDP-GlcNTFA

Prior to the start of this work, there was a chemical and enzymatic synthetic method used to produce UDP-GlcNTFA. The first step was to trifluoroacetylate GlcN-1-P, (Sigma-Aldrich), into N-acetyltrifluoroglucosamine-1-phosphate (GlcNTFA-1-P) with S-ethyltrifluorothioacetate. The second step was to combine uridine-triphosphate (UTP) and GlcNTFA-1-P to create UDP-GlcNTFA using the enzyme N-acetylglucosamine-1-phosphate uridyltransferase (GlmU).

Step 1: Synthesis of GlcNTFA-1-Phosphate from Glucosamine-1-Phosphate

The synthesis of GlcN-1-P in our lab was initially reported in 2010 (46). Eleven milligrams of GlcN-1-P were dissolved into 200µL anhydrous methanol followed by the addition 60µL of triethylamine (TEA) and 130µL S-ethyltrifluorothioacetate. The reaction was then capped and mixed via stir bar for 24 hours at room temperature. The reaction was pushed to completion by adding 50µL of S-ethyltrifluorothioacetate after 12 hours.

After 24 hours, the reaction was placed into a hood. The reaction cap was removed to allow the volatile solvent S-ethyltrifluorothioacetate to evaporate for 2 days. When complete, 200µL of water was added to the reaction and it was dried via speed vacuum overnight. Finally, 1mL of water was added and the UDP-GlcNTFA was stored.

Step 2: Enzymatic Synthesis of UDP-GlcNTFA from GlcNTFA-1-Phosphate

The second step in the synthesis of UDP-GlcNTFA was the addition of the uridine nucleotide to the GlcNTFA-1-Phosphate. A reaction was set-up containing 220µL of 2mg/mL GlcNTFA-1-P, 4µL 1M $MgCl_2$, 8µL 20mM dithiothreitol (DTT), 100µL of 100mM UTP, 100µL of 3mg/mL GlmU, 100µL of 0.1U/mL inorganic pyrophosphatase, and 800µL 25mM Tris buffer at pH 7.5. The reaction was then allowed to run for 3 hours at 30°C.

In order to verify the conversion of GlcNTFA-1-P to UDP-GlcNTFA, the final product was tested via HPLC anion exchange chromatography using a polyamine column. Sugars were eluted using a 60 minute method that provides a progressive gradient of 0-100% 1M potassium phosphate (KH_2PO_4) buffer over 40 minutes, followed by 20 minutes of 100% 1M KH_2PO_4. The HPLC analysis was also used to help determine the final product concentration using a standard curve with a UDP-GlcNAc standard. The final verification test was done via electrospray ionization mass-spectrometry (ESI-MS) analysis. All reactions completed using this method were multiples of the above concentrations.

Protein expression and purification for synthesis of UDP-glucuronic acid from glucose

Cloning of* hUDGH *DNA into pMal-c2X vector

A Human UDP-glucose dehydrogenase (hUDGH) complementary DNA (cDNA) clone was purchased, and subsequently amplified and purified. A SalI restriction enzyme (New England Biolabs) was used to cut and combine the amplified hUDGH cDNA with the chosen vector pMal-c2X (New England Biolabs). The restriction site for SalI is 5'-GTC-GAC-3'. Therefore primers were designed to amplify the hUDGH gene with the SalI restriction site using polymerase chain reaction (PCR). The forward primer was: 5' CAT-GAT-ATG-TAC-GTCGAC-TTT-GAA-ATT-AAG-AAG-ATC-TGT-TGC-3'. The reverse primer was 5'-CAT-GAT-ATG-

TAC-GTCGAC-CTA-AGA-CAC-CTT-TTT-GCC-AAT-TGT-TTC-3'. The PCR mix included 0.5µL of hUDGH cDNA template, 2.5µL of 50µM forward primer, 2.5µL of 50µM reverse primer, 5.0µL of 10X *Pfu* buffer (Agilent technologies), 0.5µL 10mM deoxynucleotide triphosphate mix (dNTP), 1.0µL *Pfu* DNA polymerase (Agilent technologies) and 37.5µL autoclaved water. The first PCR step was denaturation at 95°C for 2 minutes. Following this, there were 30 cycles of 1) denaturation at 95°C for 30 seconds, 2) elongation at 55°C for 30 seconds, and 3) annealing at 68°C for 2 minutes. The final step was annealing at 68°C for 10 minutes. The hUDGH DNA was then purified using PEG purification and PCR products verified using 1% agarose gel electrophoresis. The hUDGH DNA was then extracted from the gel via a QIAquick Gel Extraction Kit (Qiagen). Finally, it was cut with the SalI restriction enzyme, re-run on a gel, and purified via gel extraction.

A similar process also occurred for the pMal-c2X vector. While the vector was not amplified, it was cut with the SalI restriction enzyme. The vector's cut product was then verified using 1% agarose gel electrophoresis and also extracted using the QIAquick Gel Extraction Kit (Qiagen).

The pMal-c2X vector and hUDGH DNA were then ligated together using the Roche Rapid DNA Ligation Kit. In this process, 2µL of digested pMAl-c2X and 10µL of digested PCR products were mixed with 1µL T4 ligase for ligation.

Transformation of competent cells and expression cells

The ligated vector was transformed into DH5α (Invitrogen) cells. Fifty micro liters of DH5α competent cells and 1µL of the ligated DNA were placed in a 0.5mL eppendorf tube. The cells and DNA sat on ice for 30 minutes before being heat shocked at 42°C for 45 seconds. The final step was to place the mixture on ice for 2 minutes. One milliliter of sterile Luria Broth (LB)

media was then added and the cells shook at 250 RPM and 37°C for 1 hour. Afterwards, 25µL of the LB-media sample was spread on a carbenacillin 50µg/mL LB-agar plate and incubated overnight at 37°C. Several colonies were then grown in 3mL LB media and the plasmids purified using the QIAprep Spin Miniprep kit (Qiagen). Isolated plasmids were tested for vector insertion via SalI digestion and sequenced to ensure proper insertion.

The correct plasmid clones were then transformed into expressing Origami™ B (DE3) cells (Novagen) using the same transformation protocol as above. The antibiotic selection on the LB plates in this situation was 50µg/mL carbenacillin, 12.5µg/mL tetracycline and 50µg/mL kanamycin. Selected colonies were then grown in 3mL LB-media at 37°C overnight and used for expression and/or stored at -80°C with 75% glycerol for future expression.

Expression of hUDGH fused with MBP in Origami™ B (DE3) cells

A 100mL LB-media culture was started using either 15µL of stored cells containing hUDGH or 1.5mL of the aforementioned 3mL hUDGH culture. The 100mL LB media contained the same antibiotic selection as mentioned previously.

Initially the 100mL culture was used for expression of hUDGH. However, as time progressed the expression was scaled up to 6L. The expression for 6L will be discussed as this is the most recent expression. In this situation, two 100mL cultures were grown for 16-18 hours at 37°C and 220 RPM. Then 25mL of culture was added to six flasks containing 1L LB media and the aforementioned antibiotic levels.

The bacteria were allowed to grow at 37°C and 250 RPM until reaching an optical density (O.D.) of 0.6-0.8. At this time, the temperature was lowered to 22°C, and the cells were induced with 200mM Isopropyl β-D-1-thiogalactopyranoside (IPTG). After 16-18 hours the bacteria were harvested at 6000 RPM for 15 minutes until all cells had been pelleted. The

supernatant was discarded, and the pellets of bacteria were re-suspended in Buffer A for a Maltose Binding Protein (MBP) purification system that contained 25mM Tris and 500mM NaCl at a pH of 7.5. The re-suspended cells were then sonicated on ice for 30 seconds x3 at 8 output power and 50% duty cycle. The lysed cells were then spun in 40mL sonication tubes for 30 minutes at 12,000g. The supernatant was then collected and filtered through a 42.5 mm filter into 50mL conical tubes.

Purification of hUDGH fused with MBP using amylose affinity chromatography

Since hUDGH was placed into the pMal-c2X vector, the protein was expressed with a maltose binding protein. Therefore, hUDGH could be purified with amylose affinity chromatography. To collect the protein from the filtered supernatant, an amylose resin column (with size variations based on 100mL or 6L expression) was packed and washed thoroughly with Buffer A. To remove possible contaminants, the resin was then washed with the elution buffer for amylose chromatography, Buffer B, containing 25mM Tris, 500mM NaCl and 40mM maltose at pH 7.5, before having a final wash with Buffer A. Filtered supernatant was then loaded onto the column. Once added, non-binding elements were removed with Buffer A. Depending on column and expression size, 5mL or 50mL of Buffer B was then used to elute hUDGH. The protein was correctly identified using SDS-PAGE. Concentrations were determined using the nano-drop. The protein was stored without glycerol in -80°C for future use.

Cloning of LDH-Type A DNA into pET-15b vector

A human Lactate Dehydrogenase-A (LDH) clone was purchased and the cDNA was amplified and purified. NdeI and XhoI restriction enzymes (New England Biolabs) were used to cut and combine the amplified LDH cDNA and its corresponding vector, pET-15b (Novagen). The restriction site for NdeI is 5'-CAT-ATG-3', and the site for XhoI is 5'-CTC-GAG-3'.

Therefore primers were designed to amplify the LDH gene via PCR with these restriction sites in mind. The forward primer was: 5' CAT-GAT-ATG-TAC-CAT-ATG-GCA-ACT-CTA-AAG-GAT-CAG-CTG-ATT-3'. The reverse primer was 5'-CAT-GAT-ATG-TAC-CTC-GAG-TTA-AAA-TTG-CAG-CTC-CTT-TTG-GAT-CCC-3'. The reaction contained 1µL of LDH cDNA template, 2.5µL of 50µM forward primer, 2.5µL of 50µM reverse primer, 5.0µL of 10X *Pfu* buffer (Agilent technologies), 0.5µL 10mM dNTP mix, 1.0µL *Pfu* DNA polymerase (Agilent technologies) and 38µL autoclaved water. The first step of PCR was denaturation at 94°C for 2 minutes. Following this, there were 20 cycles of 1) denaturation at 94°C for 90 seconds, 2) elongation at 52°C for 90 seconds, and 3) annealing at 72°C for 210 seconds. The final step was annealing at 72°C for 10 minutes. The DNA was then purified using PEG purification and the PCR products were verified using 1% agarose gel electrophoresis. The LDH DNA was then extracted from the gel via a QIAquick Gel Extraction Kit (Qiagen). Finally, the DNA was cut with the NdeI and XhoI restriction enzymes, re-run on a gel, and purified via gel extraction. A similar process also occurred for the pET15b-vector. It was cut with the NdeI and XhoI restriction enzymes. The cut plasmid product was verified on 1% agarose gel electrophoresis and also extracted using the QIAquick Gel Extraction Kit (Qiagen).

The vector and LDH DNA were then ligated together using the Roche Rapid DNA Ligation Kit. In this process, 2µL of digested pET-15b vector and 8µL of the digested PCR LDH products were mixed with 1µL T4 ligase for ligation.

Transformation of competent cells and expression cells for LDH

For DH5α transformation, 50µL of DH5α (Invitrogen) competent cells and 10µL of the LDH ligation product were mixed in a 0.5mL eppendorf tube. The mixture sat on ice for 30 minutes before being heat shocked at 42°C for 45 seconds. The final step was to place the

eppendorf on ice for 2 minutes. Afterwards, 1mL of sterile LB media was added and the cells shook at 220 RPM and 37°C for 1 hour. Then 25µL of the media was spread on a 50µg/mL carbenacillin LB-agar plate and incubated overnight at 37°C. Several colonies were then grown in 3mL LB media and the plasmids purified using the QIAprep Spin Miniprep kit (Qiagen). Isolated plasmids were tested for vector insertion via NdeI and XhoI digestion and sequenced to ensure proper insertion.

The correct plasmid clones were then transformed into DH5α cells (Invitrogen) using the same transformation protocol as above. The antibiotic selection on the LB plates in this situation was only 50µg/mL carbenacillin. Selected colonies were then grown in 3mL LB-media at 37°C overnight and used for expression and/or stored at -80°C with 75% glycerol for future expression.

Expression of LDH-Type A in DH5α

Two 100mL LB-media cultures were started by placing 15µL of stored cells from above into each flask. The 100mL LB media also contained carbenacillin at 50µg/mL. The 100mL cultures grew for 16-18 hours at 37°C and 250 RPM. Then 25mL of culture was added to six flasks containing 1L LB media and the aforementioned antibiotic levels.

The six 1L flasks of bacteria were allowed to grow at 37°C and 250 RPM until reaching an O.D. of 0.6-0.8. At this time, the temperature was lowered to 22°C, and the cells were induced with 200mM IPTG. After 16-18 hours the bacteria were harvested at 6000 RPM for 10 minutes until all cells had been pelleted. The supernatant was discarded, and the pellets of bacteria were re-suspended in Buffer A for histidine tagged protein purification, containing 25mM Tris, 500mM NaCl, and 30mM of imidazole at pH 7.5. The re-suspended cells were then sonicated on ice for 30 seconds x3 at 8 output power and 50% duty cycle. The lysed cells were then spun in

40mL sonication tubes for 30 minutes at 11,000g. Supernatant from the lysed cells was collected and filtered through a 42.5 mm filter into 50mL conical tubes.

Purification of His_6-tagged LDH-Type A using Nickel Sepharose 6 Fast Flow™ affinity chromatography

Since the protein contained a histidine tag, the protein could be purified with nickel sepharose 6 fast flow™ affinity chromatography. To collect the protein from the filtered supernatant, approximately 20mL of nickel resin was packed into a column and washed thoroughly with Buffer A. To remove possible contaminants, the resin was then washed with the elution buffer for nickel chromatography, Buffer B, containing 25mM Tris, 500mM NaCl and 250mM imidazole at pH 7.5, before having a final wash with Buffer A. Filtered supernatant was then loaded onto the column. Once added, non-binding cell elements were removed with Buffer A. LDH was eluted with 50mL of Buffer B. The protein was correctly identified using SDS-PAGE. Concentrations were determined using the nano-drop. Collected protein was stored in 15% glycerol in -80°C for future use.

Expression of GalU

One 3mL LB-media culture was started using 15µL of stored cells containing a Glucose-1-phosphate uridyltransferase (GalU) expression vector. The 3mL culture contained carbenacillin at 50µg/mL. The culture was left to grow overnight for 16-18 hours at 37°C and 250 RPM. Then 1.5mL of culture was added to one 100mL culture containing the aforementioned carbenacillin levels.

The culture of bacteria was allowed to grow at 37°C and250 RPM until reaching an O.D. of 0.6-0.8. At this time, the temperature was lowered to 22°C, and the cells were induced with 200mM IPTG. After 16-18 hours the bacteria were harvested at 6000 RPM for 10 minutes until all cells had been pelleted. The supernatant was discarded, and the pellets of bacteria were re-

suspended in Buffer A for a histidine tagged protein, containing 25mM Tris, 500mM NaCl, and 30mM of imidazole at pH 7.5. The re-suspended cells were then sonicated on ice for 30 seconds x3 at 8 output power and 50% duty cycle. The lysed cells were then spun in 40mL sonication tubes for 30 minutes at 12,000g. Supernatant from the lysed cells was collected and filtered through a 42.5 mm filter into 50mL conical tubes.

Purification of His_6-tagged Gal-U using Nickel Sepharose 6 Fast Flow™ affinity chromatography

GalU was previously expressed with a histidine tag, and could be purified with nickel sepharose 6 fast flow™ affinity chromatography. To collect the protein from the filtered supernatant, approximately 5mL of nickel resin was packed into a column and washed thoroughly with Buffer A. To remove possible contaminants, the resin was then washed with the elution buffer for nickel chromatography, Buffer B, containing 25mM Tris, 500mM NaCl and 250mM imidazole at pH 7.5, before having a final wash with Buffer A. Filtered supernatant was then loaded onto the column. Once added, non-binding cell elements were removed with Buffer A. GalU was eluted with 5mL of Buffer B. The protein was correctly identified using SDS-PAGE. Concentrations were determined using the nano-drop. Collected protein was stored in 15% glycerol in -80°C for future use.

Protein expression and purification for PAPS-regeneration system

A 100mL LB-media culture was started using 15µL of stored cells containing Arylsulfotransferase-IV (AST-IV). The 100mL LB media contained kanamycin at 50µg/mL. The 100mL culture was left to grow overnight for 16-18 hours at 37°C and 220 RPM. Then 25mL of the 100mL culture of cells was added to three flasks containing 1L LB media and the aforementioned antibiotic levels.

The three 1L flasks of bacteria were allowed to grow at 37°C and 250 RPM until reaching an O.D. of 0.6-0.8. At this time, the temperature was lowered to 22°C, and the cells were induced with 200mM IPTG. After 16-18 hours the bacteria were harvested at 4000 RPM for 15 minutes until all cells had been pelleted. The supernatant was discarded, and the pellets of bacteria were re-suspended in Buffer A for a histidine tagged protein, containing 25mM Tris, 500mM NaCl, and 30mM of imidazole at pH of 7.5. The re-suspended cells were then sonicated on ice for 30 seconds x3 at 8 output power and 80% duty cycle. The lysed cells were then spun in 40mL sonication tubes for 30 minutes at 11,000 RPM. Supernatant from the lysed cells was then collected and filtered through a 42.5mM filter into 50mL conical tubes.

Purification of His_6-tagged AST-IV using Nickel Sepharose 6 Fast Flow™ affinity chromatography

AST-IV was previously expressed with a histidine tag. Therefore, the protein could be purified with nickel sepharose 6 fast flow™ affinity chromatography. To collect the protein from the filtered supernatant, approximately 20mL of nickel resin was packed into a column and washed thoroughly with Buffer A. To remove possible contaminants, the resin was then washed with the elution buffer for a nickel column, Buffer B, containing 25mM Tris, 500mM NaCl and 250mM imidazole at pH 7.5, before having a final wash with Buffer A. Filtered supernatant was then loaded onto the column. Once added, non-binding cell elements were removed with Buffer A. AST-IV was eluted with 20mL of Buffer B. The protein concentration was determined using the nano-drop. Protein was stored in 4gm glycerol in -80°C for future use.

CHAPTER III

Method Development: Production of UDP-GlcNTFA

As mentioned previously, UDP-GlcNTFA is a key sugar donor for the chemoenzymatic design of the HS polysaccharide chain, especially when GlcNS residues are required. In order to mimic mass production of a pharmaceutical product, it became imperative to find the most cost-effective method for acquiring UDP-GlcNTFA. The first laboratory production method required using the starting material Glucosamine-1-phosphate. However, a new option was presented in 2010 that suggested starting the process from cheaper glucosamine (47).

The complete synthesis of UDP-GlcNTFA from glucosamine

When this project started, the method for producing UDP-GlcNTFA required two steps. Briefly, the first step was the trifluoroacetylation of glucosamine-1-phosphate to create GlcNTFA-1-P. Then UTP and GlmU were added to the reaction to create UDP-GlcNTFA. However, in 2010, Zhao et. al reported using N-acetylhexosamine 1-kinase (NAHK) to create N-acetylglucosamine-1-phosphate on a large scale from N-acetylglucosamine. Therefore, we thought to use NAHK to make UDP-GlcNTFA from glucosamine, a cheaper material than glucosamine-1-phosphate. This would require two new steps in the UDP-GlcNTFA synthesis. The first step would be the trifluoroacetylation of glucosamine and not glucosamine-1-phosphate. The second step would be the phosphorylation of trifluoroacetylated glucosamine via NAHK. The last step, or the addition of uridine-diphosphate (UDP) to GlcNTFA-1-P, would remain the same. A schematic of the suggested synthetic method can be seen below (Figure 4):

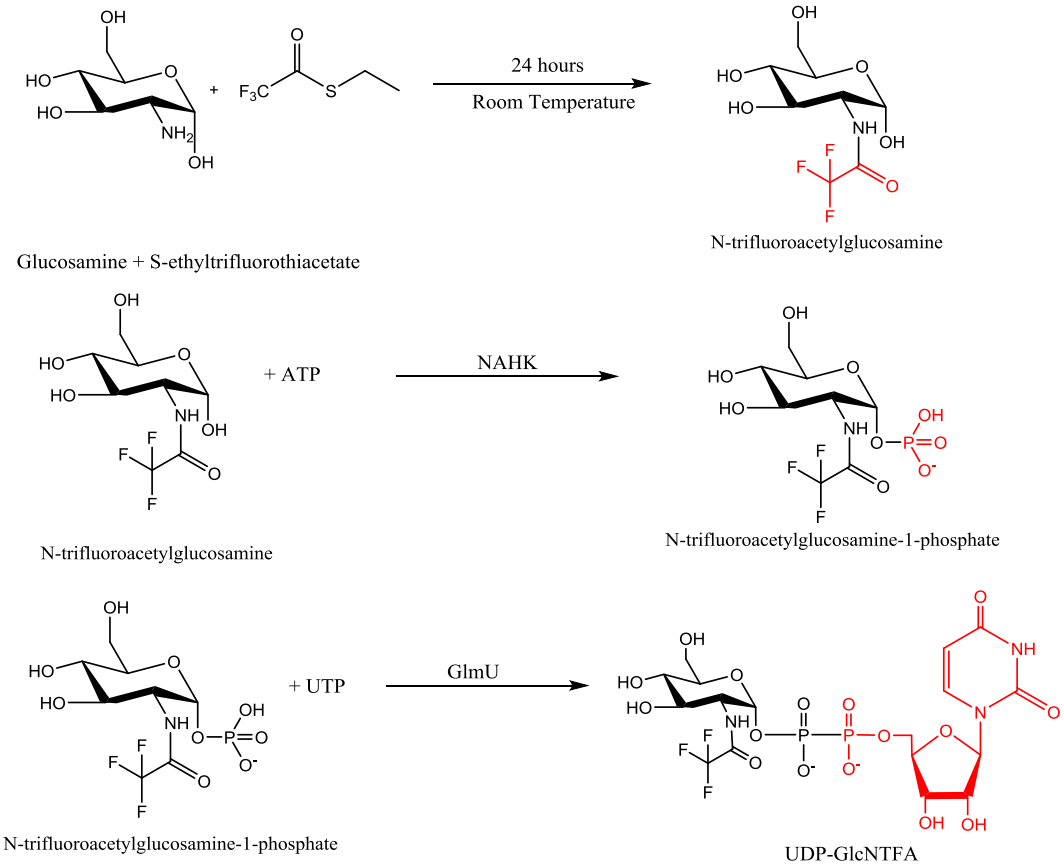

Figure 4: UDP-GlcNTFA production method proposal. This method introduced two new steps for UDP-GlcNTFA production. Note that NAHK made it possible to start from glucosamine.

Step 1: Generation of GlcNTFA from Glucosamine

The first step in this new method was to trifluoroacetylate glucosamine instead of glucosamine-1-phosphate. Initially, small reactions were used to test the process, using scaled amounts of the GlcN-1-P trifluoroacetylation method discussed in Chapter II. Note that the only way to identify successful completion of this step was to complete the entire synthesis to UDP-GlcNTFA as ESI-MS analysis of the product at this stage was inconclusive. By the end of the synthesis however, it was possible to use HPLC analysis of nucleotide depletion to test reaction completion.

After performing small scales of the reaction that were successful, the final method was set up and increased by a factor of 28. In this reaction, 300mg of glucosamine was first dissolved in 5.6mL of anhydrous methanol. Then, 1.68mL of TEA and 3.64mL of S-ethyltrifluorothioacetate were added. This was incubated in a 15mL corning tube for 24 hours. In order to drive the reaction to completion, 1.4mL of S-ethyltrifluorothioacetate was added after 12 hours.

After 24 hours the cap on the reaction tube was removed to allow for the evaporation of the volatile S-ethyltrifluorothioacetate over two days. Then 5.6mL of water was added and the reaction was allowed to dry overnight via speed vacuum to remove any additional un-evaporated reagent. When it was dry, 10mL of water was added to the reaction. The contents were then transferred to a 50mL corning tube and 18mL of water was added to give a final concentration of 49.6mM GlcNTFA, assuming 100% conversion.

Step 2: Generation of GlcNTFA-1-P from GlcNTFA using NAHK/ATP

After the first step, we tested if NAHK was capable of adding a phosphate to GlcNTFA. The reaction we mimicked was first done by Zhao et. al and contained 40mM GlcNAc, 50mM Adenosine Triphosphate (ATP),100mM Tris buffer at pH 9.0, 10mM $MgCl_2$ and 0.191mL of 1.5mg/mL NAHK brought up to a total volume of 10mL. The reaction was then incubated at 37°C for 19 hours (47).

In order to align with future HS biosynthesis, a few adjustments to this original method were necessary. In particular, there was concern of contamination of future HS biosynthetic reactions from un-reacted ATP in this step. Therefore, we reduced ATP's concentration in order to avoid contamination.

After multiple iterations of the experiment, the final reaction contained 337µmol GlcNTFA produced in step 1, 305.1µmol ATP, 9475.5µmol 1M Tris at pH 7.0, 0.015mg/mL NAHK, and 94.75µmol $MgCl_2$ in a total reaction volume of about 18mL. The reaction was incubated at 30°C for 19 hours. The final product of the reaction was thought to be GlcNTFA-1-phosphate. As with the first step, reaction success was not monitored until the last step.

Step 3: Generation of UDP-GlcNTFA via GlmU

As mentioned in the methods, this step of the process was already in place and published. However, we wanted to make sure that whatever reaction occurred, as much UTP as possible was removed in order to have a definitive quantity of UDP-GlcNTFA and to avoid any unnecessary UTP contamination. The final reaction was scaled along with the previous steps and included 76µmol of UTP, 30.81µmol of $MgCl_2$, 1.23µmol DTT, 154.05 µmol Tris at pH 7.5, ~.02mg/mL inorganic pyrophosphatase and ~0.08mg/mL of GlmU. This was allowed to run for 3 hours at 30°C. This final reaction was run on HPLC using a polyamine column and anion exchange chromatography. A sample chromatogram of sample peaks can be seen below (Figure 5):

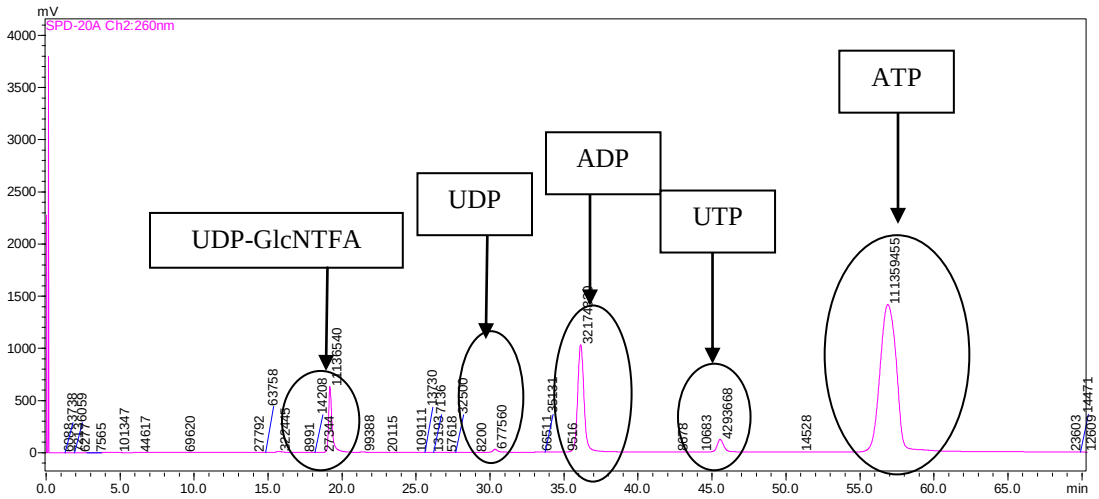

Figure 5: Chromatogram of UDP-GlcNTFA production. UDP-GlcNTFA elutes at 20 minutes. In an ideal situation, all ATP/UTP would be removed. Note that ADP represents adenosine diphosphate.

Large Scale synthesis of UDP-GlcNTFA from Glucosamine: Results

The large scale synthesis of UDP-GlcNTFA encountered a few problems by the end of the project. As mentioned, the goal was to avoid contamination with un-reacted ATP and UTP. However, there was usually a lot of ATP left in the large scale reaction, and this was unresolved by the time I completed my work on the project.

Overall, we were able to gauge the reaction's success by monitoring UTP disappearance. Full disappearance would indicate a complete reaction. The exact concentration of UDP-GlcNTFA was then determined using a UDP-GlcNAc standard.

At the end of my work on the project, one idea to improve UDP-GlcNTFA production included adding more NAHK to the reaction to drive GlcNTFA-1-P to completion with ATP before adding UTP. Note that since that time there have been many new advances that have altered UDP-GlcNTFA production from this original method.

Conclusions and Future Directions

At the end of my work on the project, we had successfully found a method to synthesize UDP-GlcNTFA from glucosamine, a cheaper starting material than glucosamine-1-phosphate. At first it was enough to support the chemoenzymatic synthesis of heparin and initial reports showed that ATP contamination may not be a significant issue. However, as HS production methods improved, a better design was necessary. In order to save time in the production of NAHK and GlmU, NAHK and GlmU were transformed and expressed into one bacterium. Additionally, cell membrane permeabilization reduced the number of steps required for UDP-GlcNTFA production from three to two. Now, glucosamine is converted to GlcN-1-P in one step and the enzymatic synthesis from GlcNTFA to UDP-GlcNTFA is another step. Current production methods create a 15mM UDP-GlcNTFA product with 70-80% yield.

CHAPTER IV[1]

Method Development: Production of UDP-GlcA

With the development of a method for UDP-GlcNTFA production, we started to examine methods to decrease the cost of UDP-GlcA. As with UDP-GlcNTFA, an option for cheaper production of UDP-GlcA presented itself in 2011 due to a report on the crystallization of hUDGH (48). With this enzyme available, a four step process for UDP-GlcA synthesis from glucose was proposed (Figure 6):

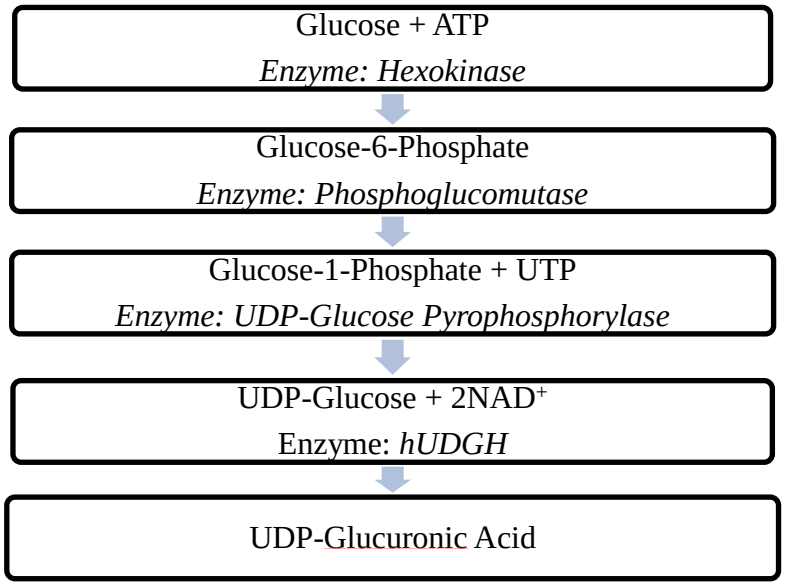

Figure 6: Schema for conversion of Glucose to UDP-Glucuronic Acid. The four steps for synthesis begin with glucose and ATP to make glucose-6-phosphate. Glucose-6-phosphate is then converted to glucose-1-phosphate using phosphoglucomutase. UDP is then added to glucose-1-phosphate via UDP-Glucose pyrophosphorylase. The final step is the oxidation of UDP-glucose to UDP-glucuronic acid via NAD^+ and the enzyme hUDGH.

[1] Portions of this chapter related to the large scale synthesis of UDP-GlcA from UDP-Glc have previously appeared in my honors thesis that was submitted to the UNC Chapel Hill University Library. The original citation is as follows: Woody, S. M. Enzymatic Synthesis of UDP-Glucuronic Acid from glucose. Honors Thesis, University Of North Carolina at Chapel Hill, 2015.

Note that the method above was developed based on previous work from the lab of George M. Whitesides. More specifically, reactions from several of his papers were adopted and then altered to create this scheme. (49-55).

Activity confirmation of hUDGH

The cloning and purification of hUDGH was discussed in the methods and was made possible due to the work of Egger and others involving their crystallization and structure analysis of hUDGH. (48, 56-58). After purification, the ability of hUDGH to covert UDP-Glucose (UDP-Glc) to UDP-glucuronic acid was tested using the reaction schema below (Figure 7):

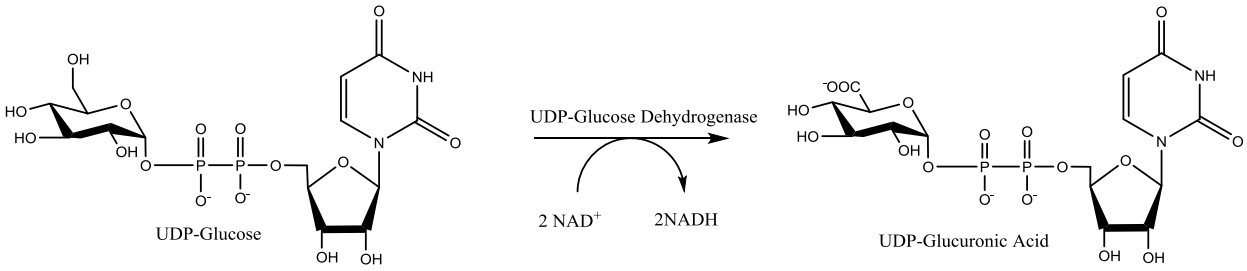

Figure 7: Conversion of UDP-Glucose to UDP-Glucuronic acid. The enzyme hUDGH is used to oxidize UDP-Glc into UDP-GlcA using 2 NAD^+. Figure adopted from (49).

More specifically, 1 equivalent of UDP-Glucose, 2 equivalents of NAD^+, and hUDGH enzyme were reacted in a total volume of 500µL. A control reaction without enzyme was also set up for comparison. The reaction was checked for completion via HPLC. Specifically, anion exchange HPLC was done using a polyamine column and a 0-100% gradient of 1M KH_2PO_4 that increased over 40 minutes running at a rate of 0.5mL/minute. Using this method, UDP-glucose elutes at 20 minutes while UDP-GlcA elutes at 30 minutes based on the UV-absorption of UDP at 260nm. Using this technique, the expressed and purified hUDGH enzyme was found to be active.

Enzymatic synthesis of UDP-GlcA from Glucose

Enzymatic synthesis of UDP-GlcA from UDP-Glc

The reaction mixture for the actual conversion of UDP-Glc to UDP-GlcA was the same as those mentioned above for testing enzyme activity. The specific components of the reaction were 0.340µM UDP-Glucose, 50µL human UDP-glucose dehydrogenase, and 1.61µM NAD^+. The mixture was brought up to a volume of 500µL using 100mM Tris Buffer at pH 8.0. The reaction was then allowed to run at 37°C overnight. The results showed incomplete activity, and were not high enough to warrant a new production method.

Upon investigation into how to make the reaction more efficient, it was found that NADH and UDP-GlcA acid are both inhibitors of hUDGH (49). Since the reaction coefficients for hUDGH were 1:2 in favor of NAD^+ there was a strong concern for product inhibition. However, previous work had shown the effectiveness of an NAD^+ regeneration system that would avoid excessive NADH production (49).

NAD^+ Regeneration System

As mentioned previously, a two to one ratio of NAD^+ to UDP-Glc was necessary for conversion of UDP-Glc to UDP-GlcA. The cost of NAD^+, plus NADH product inhibition were both concerning for method development. However, previous works had a similar problem and offered a novel solution. Specifically, in the work of Toone and colleagues, UDP-Glc to UDP-GlcA conversion was only 10% after several days (49). Although it was not what they considered their primary issue, the authors did note that NADH could be an inhibitor of UDGH. Therefore, they suggested an NAD^+ regeneration system using LDH to improve their reaction yield (Figure 8):

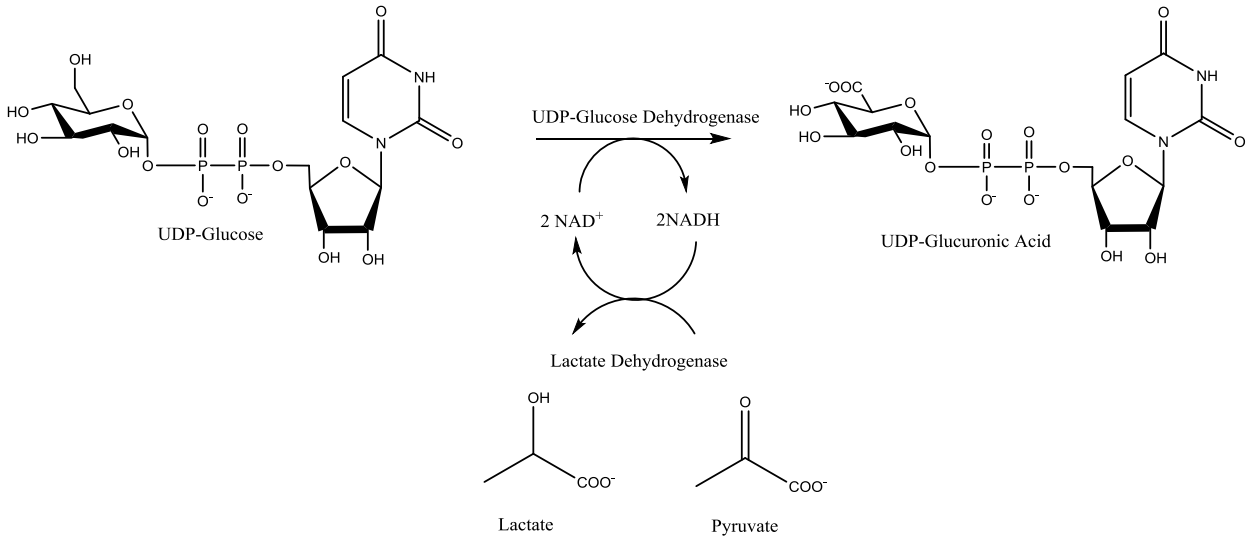

Figure 8: Conversion of UDP-Glc to UDP-GlcA with the NAD^+ regeneration. In this system, NAD^+ is regenerated using pyruvate and lactate dehydrogenase. An excess of pyruvate is added to drive the regeneration system allowing for full UDP-Glc conversion to UDP-GlcA. Figure adapted from (49).

Note that in addition to adding the NAD^+ regeneration system, the authors also changed their source of UDGH as they also experienced enzyme degradation. Together, these two changes increased their recovery to 87% (49).

Based on their success, a NAD^+ regeneration system was added to our reaction. The first reaction protocol included 0.170µM NAD^+, 3.7mM pyruvate, 50µL hUDGH, .340µM UDP-GlcA, and 5 units (U) of lactate dehydrogenase (LDH) purchased from Sigma-Aldrich. The reaction was allowed to incubate at 37°C overnight. The reaction was checked for completion via HPLC as mentioned previously. Again, UDP-glucose in this setting is eluted at 20 minutes while UDP-GlcA elutes at 30 minutes based on the UV-absorption of UDP at 260nm. This process led to 100% conversion of UDP-Glc to UDP-GlcA as seen below (Figure 9):

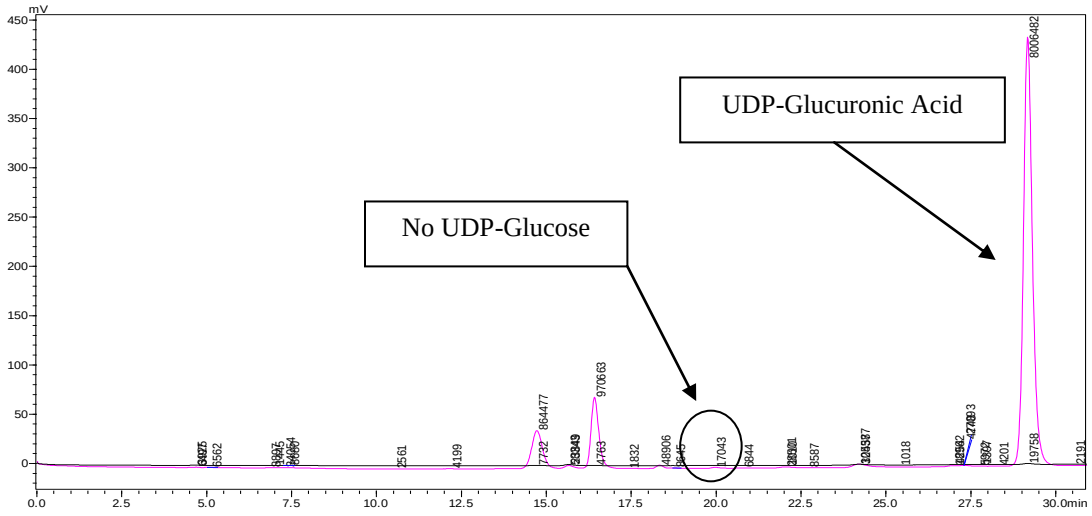

Figure 9: Chromatograms of UDP-Glc conversion to UDP-GlcA. The lack of a peak at 20 minutes shows that all UDP-Glc was converted to UDP-GlcA, which elutes at 30 minutes.

.

Enzymatic Synthesis of UDP-GlcA from Gucose-1-Phosphate

Upon successful conversion of UDP-Glc to UDP-GlcA, the next step was to start the process from glucose-1-phosphate (Glc-1-P) using Uridine-5'-diphosphoglucose pyrophosphorylase (UDP-Glc PPase) and UTP. This enzyme catalyzes the reaction as seen below (Figure 10):

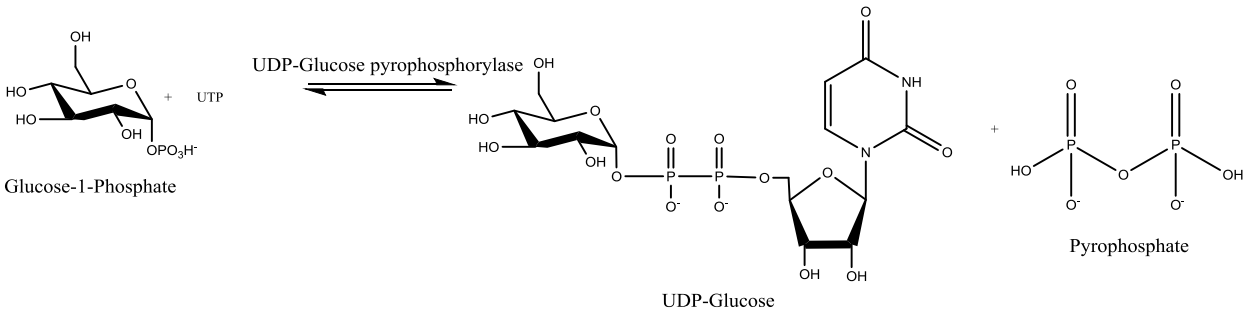

Figure 10: Conversion of Glc-1-p to UDP-Glc. UDP-Glucose pyrophosphorylase catalyzes the reaction of Glc-1-P and UTP to UDP-glucose. Note that since the reaction is reversible, inorganic pyrophosphatase is added to remove inorganic pyrophosphate and drive the reaction forward.

In order to start from glucose-1-phosphate, UDP-Glc-PPase, UTP, and inorganic pyrophosphatase were added to the initial conditions. The new reaction mixture contained 0.170µM NAD^+, 3.7mM pyruvate, 50µL UDP-glucose dehydrogenase, 5U LDH (Sigma-

Aldrich), 200U UDP-Glc PPase (Sigma Aldrich), 1mM glucose-1-phosphate, 2mM UTP, 5µM $MgCl_2$, and 1µL inorganic pyrophosphatase. Excess UTP was added to ensure reaction completion. The reaction was then allowed to incubate at 37°C overnight. Again, reaction completion was checked via HPLC with UDP-GlcA elution at 30 minutes. Two other peaks that appeared in this reaction were UTP and UDP. UDP elutes at about 30 minutes (typically following UDP-GlcA) and UTP elutes at about 50 minutes. Starting from glucose-1-phosphate using these conditions led to conversion of Glc-1-P to UDP-GlcA as seen below (Figure 11):

A) Reaction from Glucose-1-Phosphate: Reaction

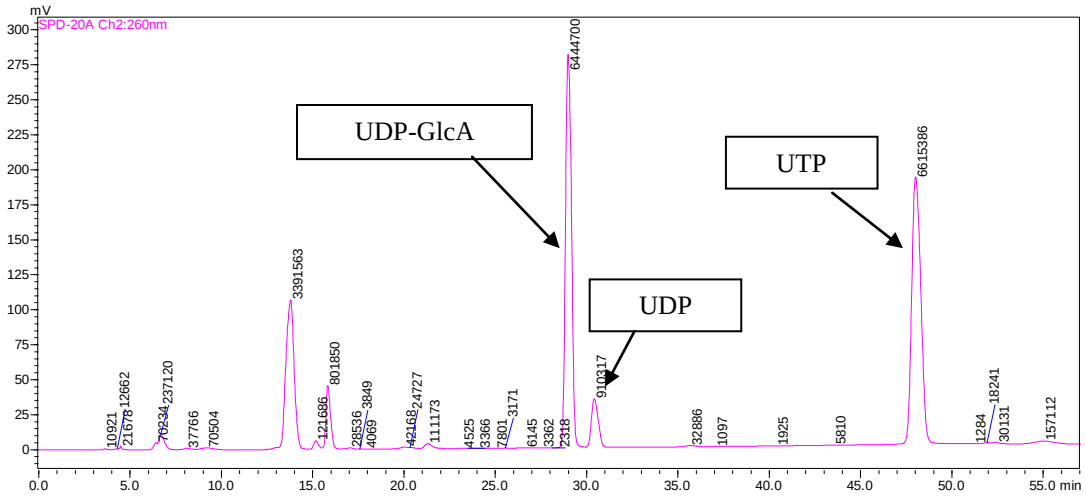

B) Reaction from Glucose-1-Phosphate: Control

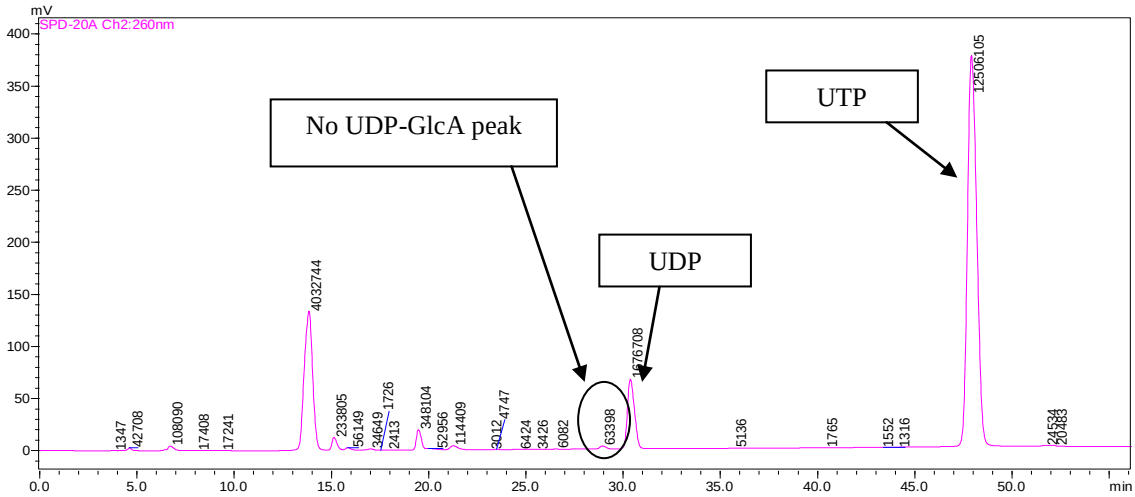

Figure 11: Chromatograms of the conversion of Glc-1-P to UDP-GlcA. (A) represents the experimental reaction and (B) represents the control. The presence of the UDP-GlcA peak at 30 minutes in (A) shows that the Glc-1-P was successfully converted to UDP-GlcA. The peak at 30 minutes from (B) is UDP, and likely represents UTP degradation as it is also seen in the enzyme reaction (A). The excess UTP in (A) is expected based on reaction conditions of 1mM Glc-1-P to 2mM UTP

Enzymatic Synthesis of UDP-GlcA from Gluocse-6-Phosphate

For the third step, the requirements for the synthesis of UDP-GlcA from glucose-6-phosphate (Glc-6-P) included the addition of phosphoglucomutase (PGM). This enzyme catalyzes the reaction as seen below (Figure 12):

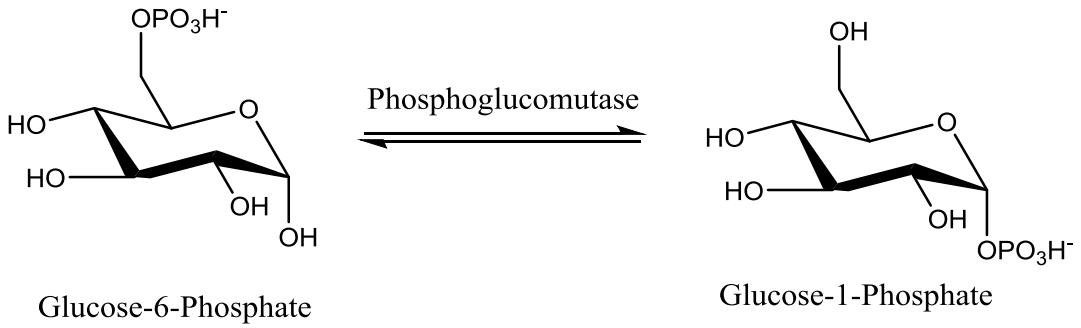

Figure 12: Conversion of Glc-6-P to Glc-1-P: This is the conversion between glucose-6-phopsphate and glucose-1-phosphate.The reaction favors the glucose-6-phosphate direction, so glucose-1-phosphate must be consumed to push the reaction forward.

In order to start from glucose-6-phosphate, phosphoglucomutase was added to the reaction starting from Glc-1-P. PGM tends to favor the formation of Glc-6-P over Glc-1-P, making the presence of subsequent reactions that use Glc-1-P absolutely necessary in order to drive the reaction forward. For this reaction the components were 0.170µM NAD^+, 3.7mM pyruvate, 50µL UDP-glucose dehydrogenase, 5U LDH (Sigma-Aldrich), 200U UDP-Glc PPase (Sigma Aldrich), 1mM glucose-6-phosphate, 2mM UTP, 5µM $MgCl_2$, 1µL inorganic pyrophosphatase, and 50U PGM (Sigma Aldrich). As with before, excess UTP was added to ensure reaction completion. The reaction was then allowed to incubate at 37°C overnight. Reaction completion was checked via HPLC as was done previously, with the same elution times. The initial results for this reaction were also promising as seen below (Figure 13):

A) Reaction from Glucose-6-Phosphate: Reaction

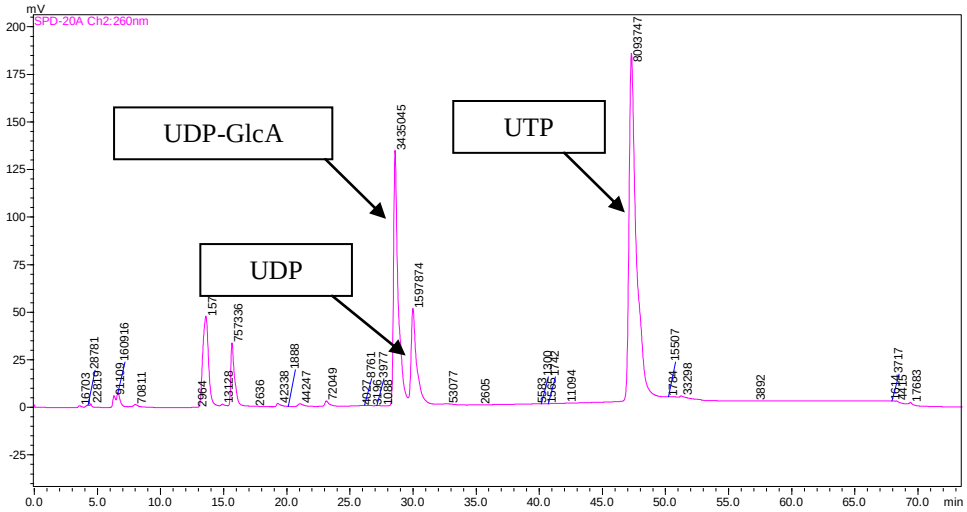

B) Reaction from Glucose-6-Phosphate: Control

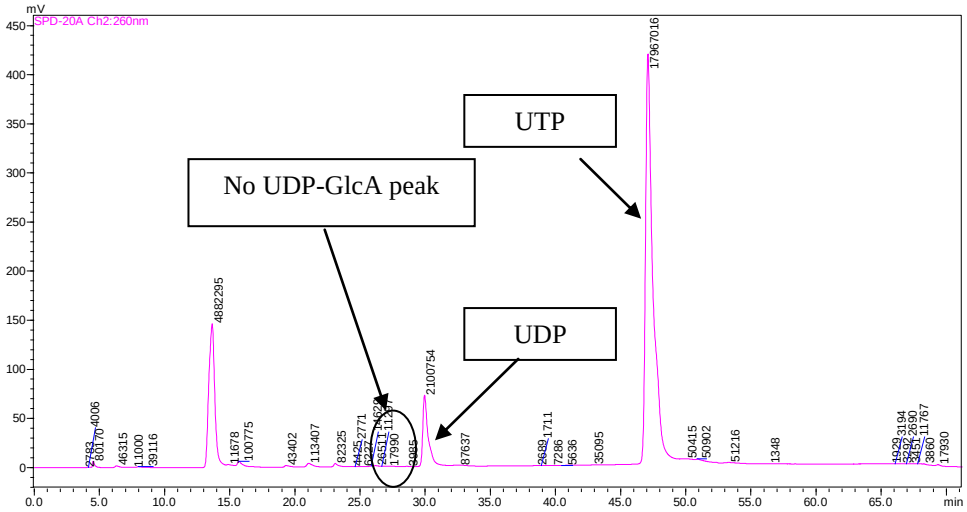

Figure 13: Chromatograms of the conversion of Glc-6-P to UDP-GlcA. (A) represents the experimental reaction and (B) represents the control. The presence of the UDP-GlcA peak at 30 minutes in (A) shows that the Glc-6-P was successfully converted to UDP-GlcA. The peak at 30 minutes from (B) is UDP, and likely represents UTP degradation as it is also seen in the enzyme reaction (A). The excess UTP in (A) is expected based on reaction conditions of 1mM Glc-6-P to 2mM UTP.

Enzymatic Synthesis of UDP-GlcA from Glucose

For the final synthetic step, hexokinase was the enzyme of choice as it catalyzes the reaction below (Figure 14):

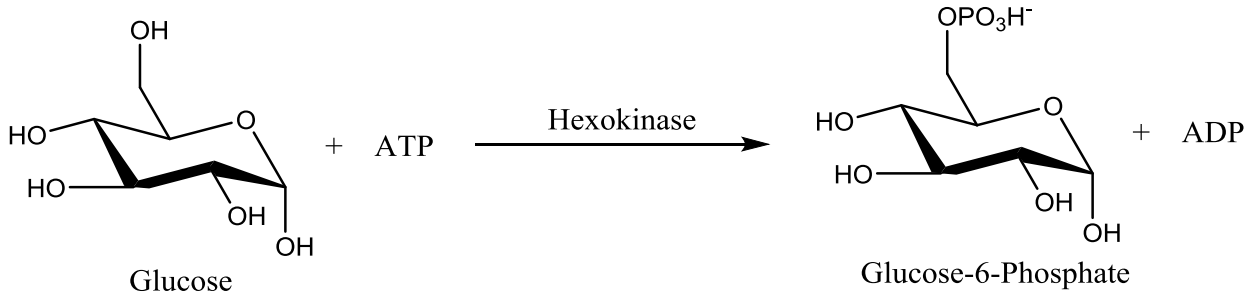

Figure 14: Conversion of Glucose to Glucose-6-Phosphate. This is a one way reaction where hexokinase uses ATP and glucose to create Glc-6-P.

The final addition to the reaction was hexokinase and ATP. Conditions for the hexokinase reaction were based off of kinetic and activity studies of various hexokinases. (59-62). Therefore the final reaction included 0.170µM NAD^+, 3.7mM pyruvate, 50µL UDP-glucose dehydrogenase, 5U LDH (Sigma-Aldrich), 200U UDP-Glc PPase (Sigma Aldrich), 1mM glucose, 2mM UTP, 1mM ATP 5µM $MgCl_2$, 1µL inorganic pyrophosphatase, 50U PGM (Sigma Aldrich), and 10µL hexokinase (Sigma-Aldrich). The reaction was then allowed to incubate at 37°C overnight. Reaction completion was checked via HPLC as was done previously, with the same elution times. Two additional peaks in this spectrum included ATP and ADP. ADP elutes at about 35 minutes and ATP at about 60 minutes based on adenine UV-absorbance at 260nm. This last step was successful, but the hexokinase reaction could not be confirmed 100% due to the presence of leftover ATP. Moreover, the peak areas for ATP and UTP compared to the control suggested a possible lack of enzyme specificity (Figure 15):

A) Reaction from Glucose: Reaction

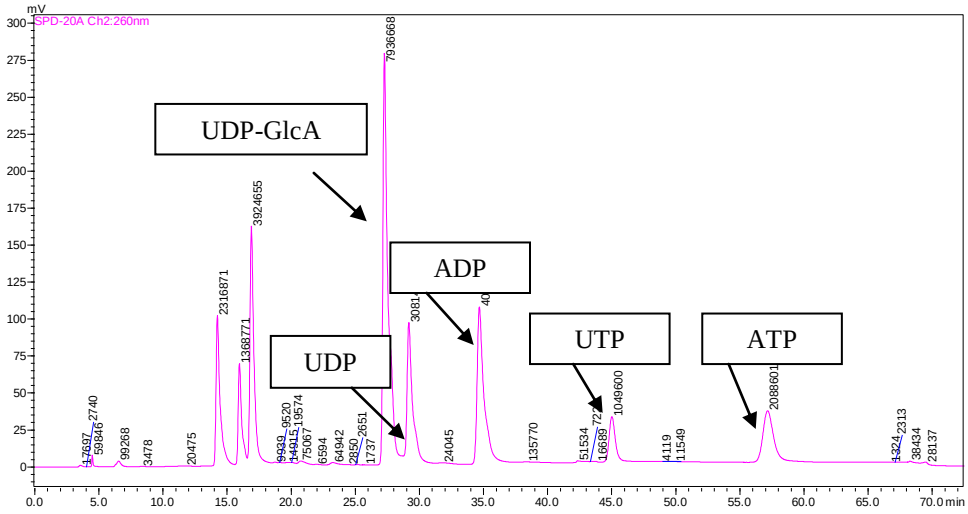

B) Reaction from Glucose: Control

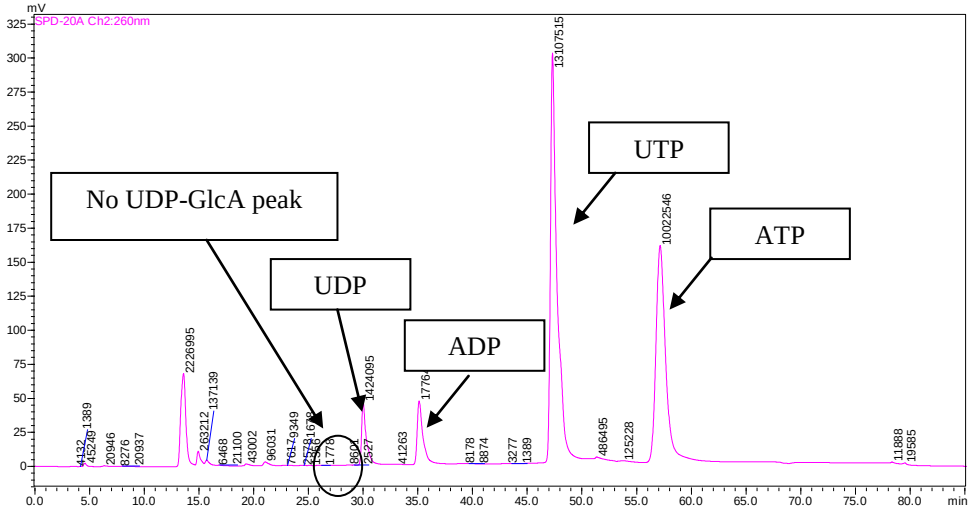

Figure 15: Chromatogram of the conversion of Glucose to UDP-GlcA. (A) represents the experimental reaction and (B) represents the control. The presence of the UDP-GlcA peak at 30 minutes in (A) shows that the glucose was successfully converted to UDP-GlcA. The peak at 30 minutes from (B) is UDP, and likely represents UTP degradation as it is also seen in the enzyme reaction (A). The excess UTP in (A) is expected based on reaction conditions of 1mM glucose to 2mM UTP. However, the excess ATP is not expected and equivalent peaks between UTP and ATP in (A) suggests a lack of enzyme specificity when distinguishing between ATP and UTP.

We tried extending the reaction and lowering the UTP concentration from 2mM to 1mM to force the reaction forward, and while this helped, the results about completion were inconclusive.

Heparin elongation using enzymatically synthesized UDP-GlcA

With the success of the first three steps of our reaction, we wanted to make sure that we could use our UDP-GlcA product in heparan sulfate chemoenzymatic synthesis. Since there was concern about ATP/ADP interference with elongation, we used the procedure from glucose-6-phoshate to UDP-GlcA that only required UTP, to create our UDP-GlcA starting material. After the reaction was complete we spun it down and performed an elongation reaction with 100µg disaccharide, ~half of our reaction sample, and 100µL pmHS2. This was then allowed to run overnight. The pmHS2 was able to use our UDP-GlcA product as was determined via ESI-MS (Figure 16):

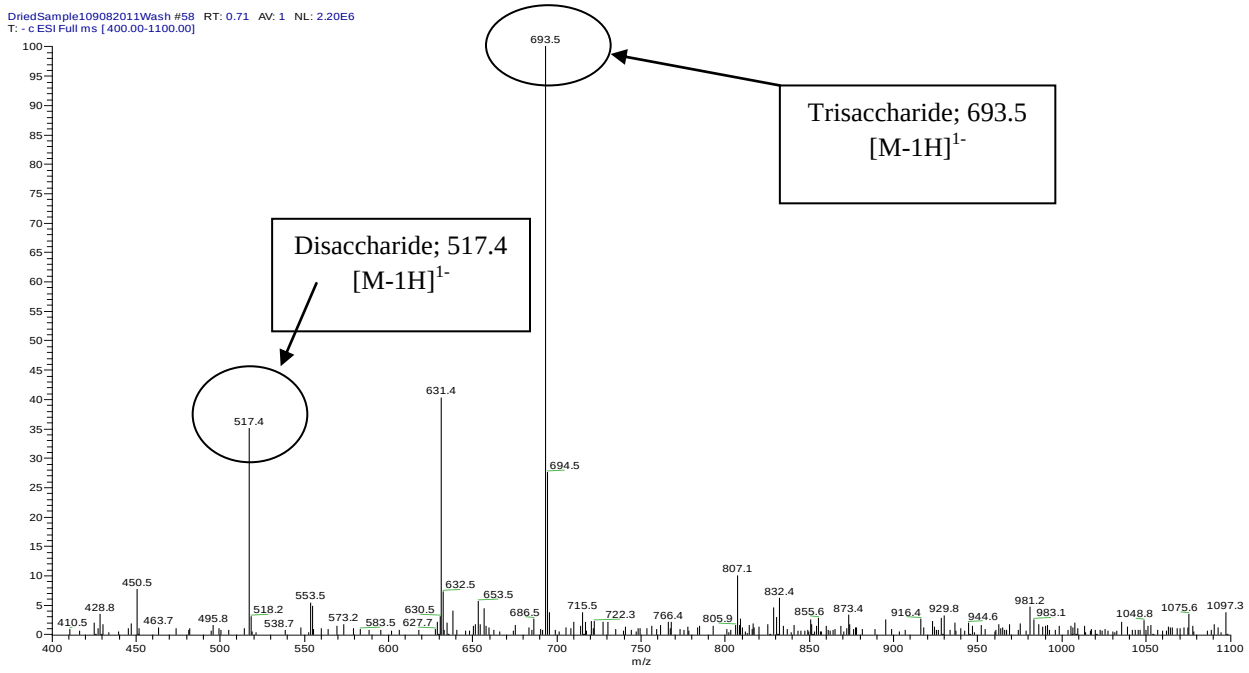

Figure 16: ESI-MS of PNP-GlcA-GlcNac-GlcA. The molecular weight of the disaccharide that started the reaction was 518.14. The molecular weight of the expected trisaccharide was expected to be 694.17. The associated *m/z* ratios would be 517.14 and 693.14 and were confirmed via ESI-MS.

Activity confirmation of LDH-Type A

As the potential for the synthesis of UDP-GlcA in-house became possible, the production of the enzymes purchased from Sigma-Aldrich was necessary. Reports on the successful

expression of a human LDH complementary DNA (63-64) led to the in-house cloning and expression of human-LDH-A4. In order to test for activity, the ability of in-house LDH to support the regeneration system was tested and proven successful.

UDP-pyrophosphorylase/GalU

Many attempts were made to clone and express yeast UDP-Glc PPase based on literature reports since it would be equivalent to what was purchased from Sigma Aldrich (65-66). After several unsuccessful attempts, a bacterial glucose-1-phosphate uridyltransferase (GalU) was used as a replacement for the purchased yeast UDP-Glc PPase. GalU's ability to convert glucose-1-phosphate to UDP-Glucose was used to test its activity. While GalU was effective, its stability was initially not the same as compared to the purchased UDP-Glc PPase. Therefore, until such time as this issue could be resolved, we only produced UDP-GlcA from UDP-Glc due to its high completion rate and the successful expression of both LDH and hUDGH.

Large scale synthesis of UDP-GlcA from UDP-Glc

As the glucose to UDP-GlcA reaction progressed, it was necessary to mass produce UDP-GlcA at levels required for HS biosynthesis for as cheap as possible. The most successful reaction at this point was UDP-Glc to UDP-GlcA as mentioned previously. UDP-Glc is four times cheaper than UDP-GlcA so we began a mass production method for UDP-GlcA (67). Overall, the reaction size was increased to produce approximately 100mg of UDP-GlcA. The reaction contents were 1.6mL of 0.1M UDP-Glucose, 52µL of 0.15M NAD^+, 1.4mL of 1M pyruvate, 260µL of 1M $MgCl_2$ and 23mL of 50mM Tris buffer at pH 8.5. The enzymes used for the reaction included the hUDGH and LDH made in house. The concentrations for LDH and hUDGH varied per expression period, but each generally had a concentration greater than a

1mg/mL. In all reaction schemas, 2mL of hUDGH and 260µL of LDH were used despite the exact concentration.

To purify the UDP-GlcA, the reaction was loaded onto a Q-sepharose affinity chromatography column. UDP-GlcA was then isolated by attaching the Q-sepharose column to the HPLC and using a 0-100% high salt elution method and 1mL/min flow rate. As can be seen below, the resulting product was off the scale of the HPLC UV-Vis (Figure 17):

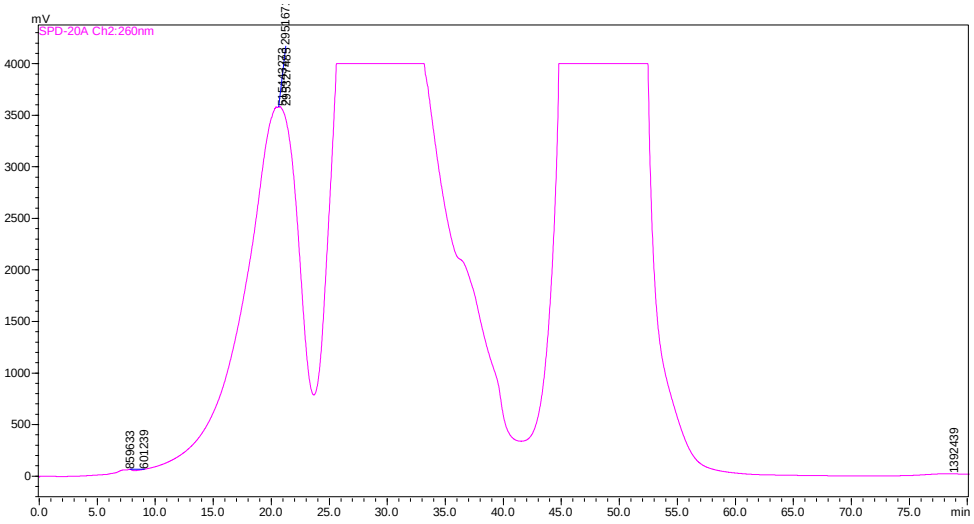

Figure 17: Chromatogram of Q-Sepharose Elution UDP-GlcA large scale elution demonstrates that absorbance is unreadable by the HPLC UV-Vis detector. Therefore, to collect fractions containing the most UDP-GlcA, absorbance was determined by diluting individual fractions and collecting those with the highest absorbance.

Based on previous work, the UDP-GlcA elution was at about 50 minutes. Therefore, elution fractions around this time were collected and their UV-Vis absorption was manually re-measured after a 1000x dilution. Generally, fractions that read above a 0.2 absorbance unit after dilution were pooled together. The final concentration of UDP-GlcA was then determined by a UDP-GlcA standard curve.

Tracking the reaction progression and completion

To determine the success of the reaction from UDP-Glc to UDP-GlcA, the complete removal of UDP-glucose was monitored on the HPLC. The process was generally very effective

with almost 100% yield as mentioned previously. However, after conversion, there was still a potential for loss during the purification of UDP-GlcA. Therefore, a verified UDP-GlcA concentration after purification was necessary using a UDP-GlcA standard curve created via HPLC. The standard curve used UDP-GlcA concentrations 10x more dilute than the final reaction in order to visualize the UDP-GlcA without going past maximum absorbance. The creation of this standard curve can be seen in Table 2 and Figure 18:

Concentration	Area under the peak
0µM	------
1µM	41785070
2µM	55275462
3µM	72737178
4µM	84067050
5µM	111969240
6µM	117900535

Table 2: **UDP-GlcA HPLC Areas.** The standard curve concentrations and associated areas under the peak after HPLC analysis using anion exchange chromatography and the polyamine column with a 0-100% gradient of 1M KH_2PO_4 over 40 minutes.

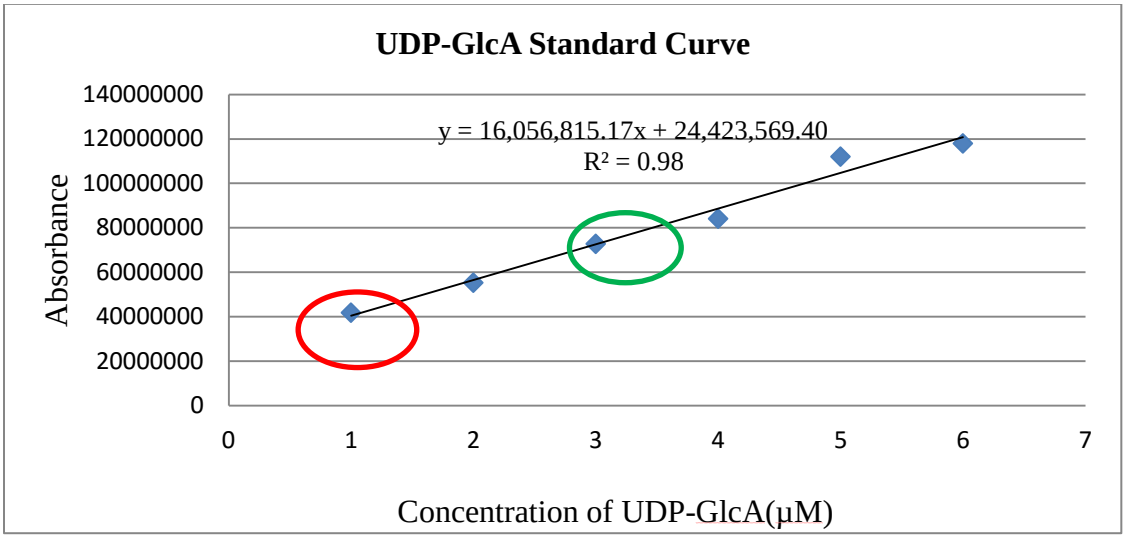

Figure 18: Standard curve of UDP-GlcA concentration. Standard curve of UDP-GlcA created using concentrations 10X less than what was expected. The expected concentration of UDP-GlcA from large scale synthesis size is shown in the green circle, and the actual concentration is shown in the red circle.

Purification of UDP-GlcA on a large scale

As the reaction scale was increased to amounts larger than 100mg, there was some loss of product from purification, but generally we expected an 80-90% yield. However, when we attempted to purify a reaction that had started with 1.25grams of UDP-Glc, our yield was much lower. Instead of an 80-90% yield after purification, there was only a 40-50% yield. In Figure 18, the expected concentration of UDP-GlcA after purification is in green and the actual final concentration after purification is in the red circle. As demonstrated by these differences in absorption, there was a significant loss of UDP-GlcA.

As part of the trouble-shooting process to find the missing product, the flow through from the Q-sepharose column was run on the HPLC to determine the amount of wasted material. The result can be seen in Figure 19:

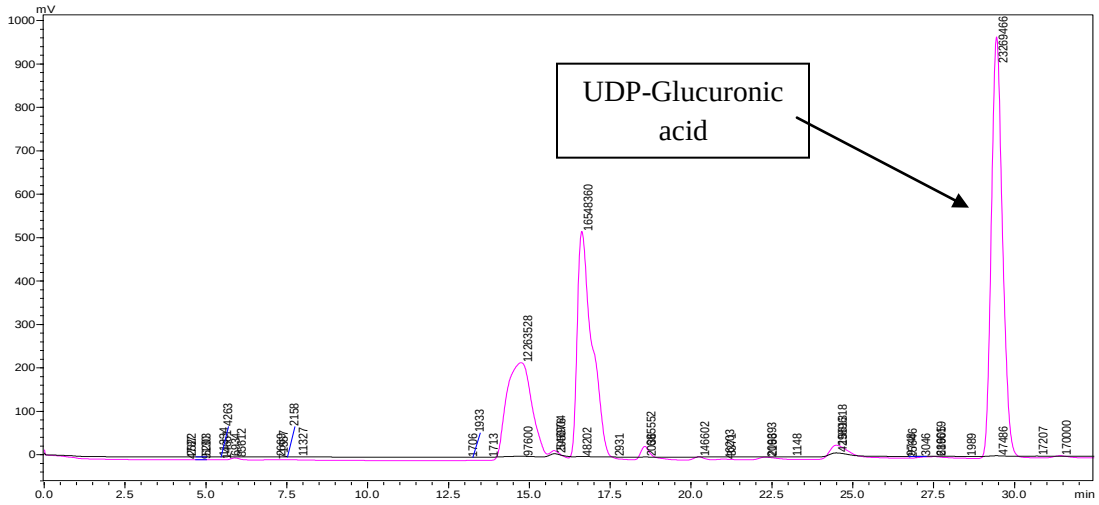

Figure 19: Chromatogram of flow through of Q-sepharose purification. The presence of a peak at 30 minutes shows that UDP-GlcA is present and did not bind to the column, suggesting inadequate Q-sepharose binding capacity.

As demonstrated above, the flow through did contain UDP-GlcA, and we found it to be about 0.25 grams, or 18% of the expected UDP-GlcA sample. This indicated that there was significant loss upon purification with the Q-sepharose column.

Therefore, the loading capacity of the Q-sepharose column was checked to make sure it could take the amount of sample loaded. It was then discovered that the column had a maximum loading capacity for UDP-GlcA of about 1 gram. Assuming 100% conversion of 1.25grams of UDP-glucose to UDP-GlcA, ~1.4grams of UDP-GlcA was loaded onto the column. Therefore, not all of the UDP-GlcA was able to bind to the column for subsequent elution and collection.

Afterwards two strategies were implemented to help avoid over-loading the Q-sepharose column. Less material was loaded onto the existing column, and we started to use larger Q-sepharose columns with larger binding capacities to load and purify larger amounts of UDP-GlcA.

Conclusions and future directions

Using the above methodologies, we were able to create a unique method to convert glucose into UDP-GlcA. However, for the purposes of synthesizing UDP-GlcA, at the end of my work on the project, starting from UDP-glucose was the best option, as the price was four times cheaper than UDP-GlcA (67). Due to the success of converting UDP-Glc to UDP-GlcA, and the precipitation propensity of hUDGH, this step was never placed back into the original one-pot reaction. Instead, it has remained a separate step.

Future goals of this project at the end of my work were to create a two-step reaction with one pot converting glucose to UDP-glucose and the other pot converting UDP-Glc to UDP-GlcA. Moreover, our lab wanted to successfully clone and express all necessary enzymes in-house.

In order to follow through with these goals, a cell permeabilization method for UDP-GlcA production was created. In this technique, there are two sets of bacteria called Set1 and

Set2 containing all of the enzymes necessary for the conversion of glucose to UDP-Glc. As was done with UDP-GlcNTFA, the cells are permeabilized and all necessary non-enzymatic reactants are added. After a specified interval, the supernatant of the cells is then isolated and combined with hUDGH, LDH, NAD^+, and pyruvate to generate UDP-GlcA. We then purify UDP-GlcA using affinity chromatography. The total yield is about 70-80% using this method.

CHAPTER V

Method development: PAPS Regeneration System

Even with the success of the starting material synthesis, there are still barriers to HS polysaccharide mass production. Specifically, as the polysaccharide size increases, certain modifications become more difficult to drive to completion. Therefore, there is a mixture of products, although they can typically be separated to greater than 99% purity (40). The incomplete reactions could theoretically be due to product or by-product inhibition, but the exact cause remains unclear and is an area for improvement.

Activity confirmation of AST-IV

Arylsulfotransferase-IV (AST-IV) has been used to donate a sulfur group from paranitrophenol sulfate (PNPS) to PAP as seen below (2) (Figure 20):

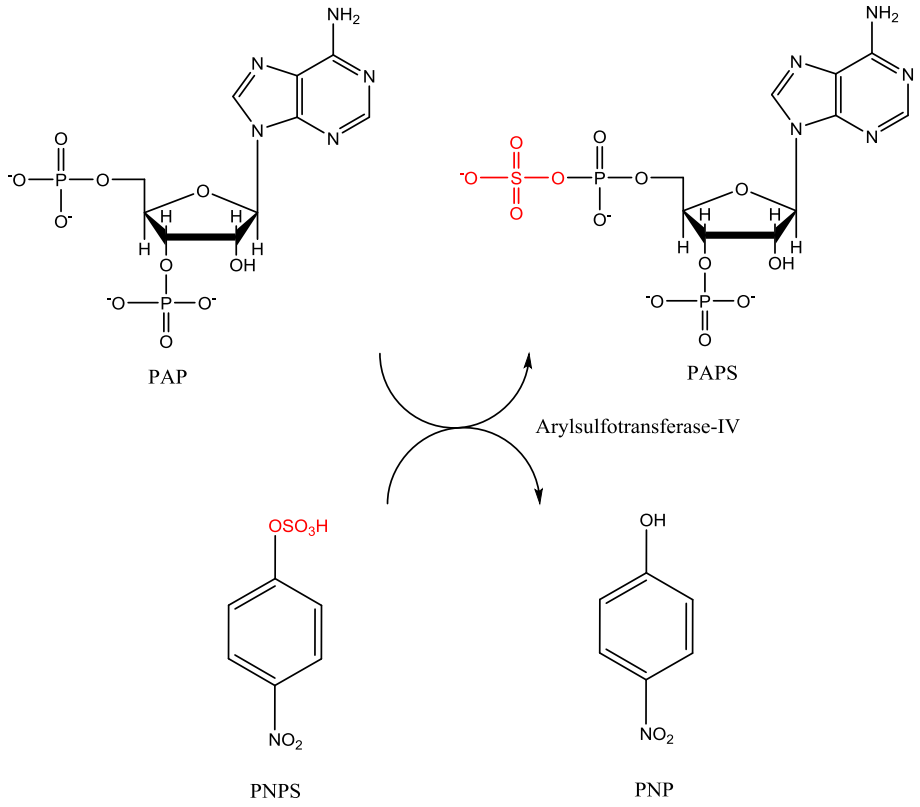

Figure 20: AST-IV reaction schema. A sulfate group from PNPS is given back to PAPS via the enzyme Arylsulfotransferase-IV. The by-product of the reaction is paranitrophenol (PNP), and has a yellow tint when in a clear solution. Figure adapted from (2).

During this conversion, paranitrophenol (PNP) is released and will alter the color of the clear reaction mixture to yellow. Therefore, in order to verify AST-IV activity, two reactions were carried out to verify that it worked. The successful reaction can be seen below (Figure 21):

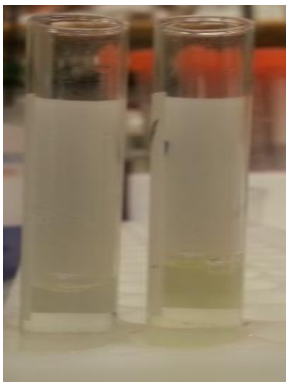

Figure 21: AST-IV activity confirmation. The by-product of the AST-IV reaction is PNP, and has a yellow tint to it when in a clear solution. The solution on the right in the above picture has AST-IV compared to the solution on the left that does not have AST-IV. The yellow tint indicates active AST-IV.

Regeneration of PAPS from PAP using AST-IV and PNPS in a 6-OST-3 system

AST-IV has previously been reported as a method to regenerate PAPS (2), and therefore may play a role in current chemoenzymatic synthesis techniques. One way to drive incomplete HS polysaccharides reactions, such as 6-O-sulfation of higher order polysaccharides, is to dilute the reaction and add more PAPS. Since dilution was necessary, it was thought that there may be some product inhibition of the HS enzymes by PAP. One way to overcome this issue would be to reduce the total amount of PAPS used in the sulfation reactions, and therefore lower the PAP concentration. A possible method to lower the PAP concentration, similar to the NAD^+ regeneration system, would be to add a PAPS regeneration system using PNPS and AST-IV. In order to do this, the first step was to determine the optimal concentration of PNPS for PAPS regeneration.

Optimal concentrations of PNPS for PAPS regeneration and AST-IV inhibition

As was mentioned with the NAD^+ regeneration system, an excess of the reactant in the regeneration system is necessary for optimal regeneration. Therefore we tested the regeneration system using a partially sulfated hexasaccharide that needed 6-O-sulfation at three locations. The compound was the result of an incomplete 6-O-sulfation reaction. The completely sulfated product had already been moved forward in the HS polysaccharide synthesis. The reaction started with a mixture of 0.250mM hexasaccharide, 0.250mM PAPS, and 6-OST-3 that was placed in a 30°C water bath for one hour. Then AST-IV and either a 1X, 3X, or 5X concentrations of PNPS were added to the reaction. The reaction then remained at 30°C overnight. To check for completion, the reaction was analyzed using HPLC and anion exchange chromatography via polyamine column. The flow was set to 1mL/min using a high salt elution with a 0-100% KH_2PO_4 gradient over 20 minutes. Absorption was detected via the PNP-tag on

the oligosaccharide which has UV-Vis absorbance at 310nm. The more sulfation present on the compound, the longer the retention time, with all compounds eluting between 15-20 minutes. Based on this analysis, initially, the reaction appeared to be successful (Figure 22):

A) 1X PNPS

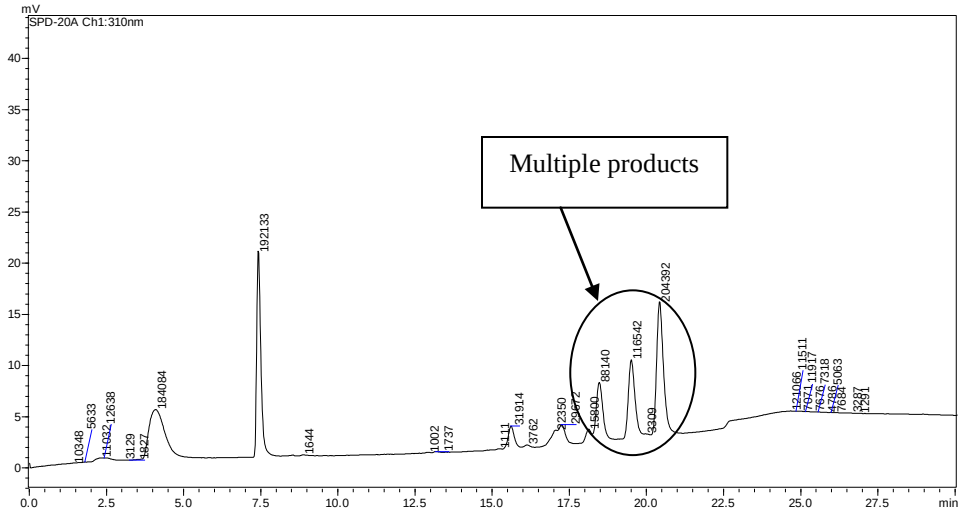

B) 5X PNPS

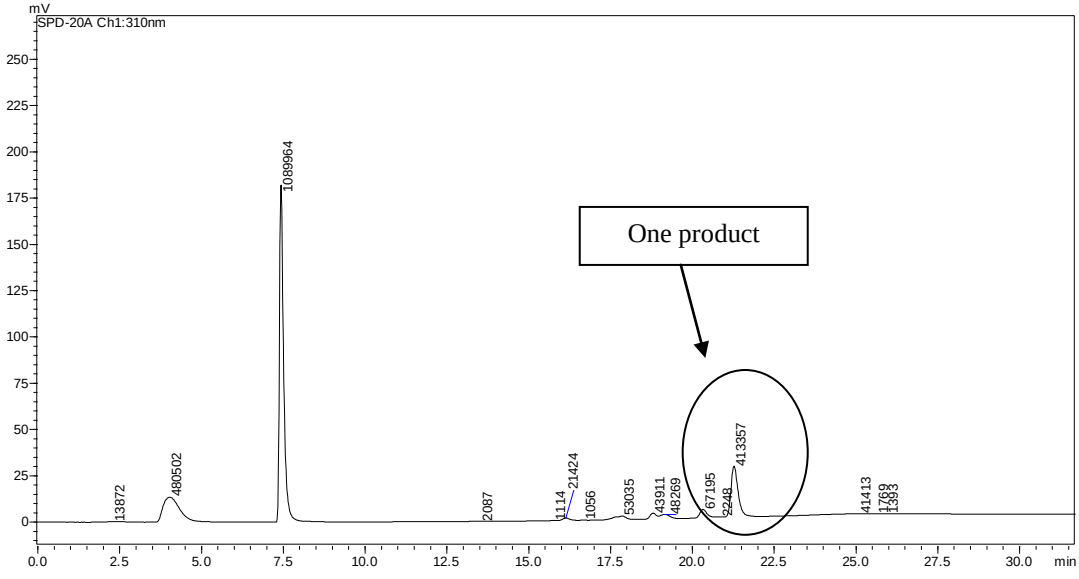

Figure 22: Chromatogram of AST-IV Regeneration System: (A) represents a chromatogram of the reaction with partially sulfated 0.250mM hexasaccharide, 0.250mM PAPS, and 6-OST-3 that included 0.250mM PNPS and AST-IV for regeneration. (B) represents a chromatogram of the reaction with partially sulfated 0.250mM hexasaccharide, 0.250mM PAPS, and 6-OST-3 that included 1.25mM PNPS and AST-IV for regeneration. Results from (A) suggest incomplete sulfation as there are multiple sulfated products, while the results from (B) show only one sulfated product, and indicate a complete reaction.

While the reaction appeared to be successful using 5X PNPS, the scale would need to be increased to 2-4mM of compound in order to mimic the normal HS synthesis.

Inhibition of AST-IV by PAP/PAPS

The next step was therefore to scale up the reaction. However, when the concentration of the hexasaccharide was increased the reaction was not successful when analyzed via HPLC. Moreover, the results from the first reaction did not seem to be repeatable (Figure 23):

A) 0.250mM hexasaccharide

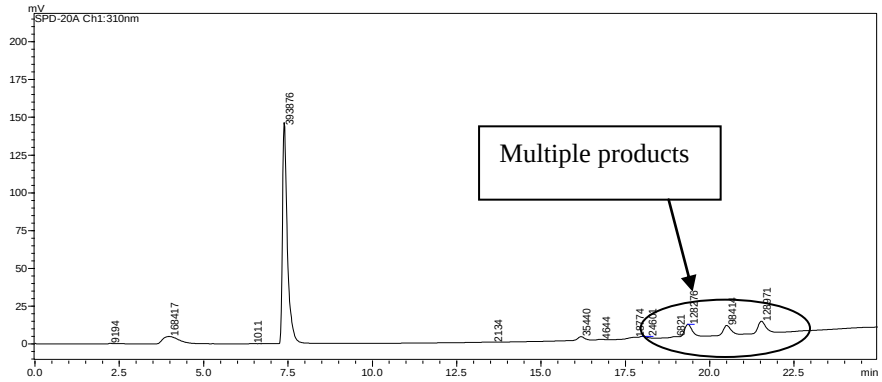

B) 0.750mM hexasaccharide

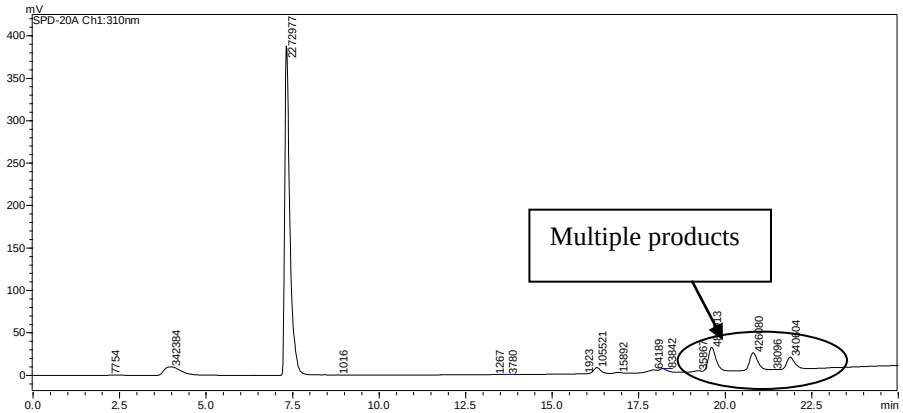

Figure 23: Chromatogram of Scaled AST-IV Regeneration System: (A) represents a chromatogram of the reaction with partially sulfated 0.250mM hexasaccharide, 0.250mM PAPS, and 6-OST-3 that included 1.25mM PNPS and AST-IV for regeneration. (B) represents a chromatogram of the reaction with partially sulfated 0.750mM hexasaccharide, 0.750M PAPS, and 6-OST-3 that included 3.75mM PNPS and AST-IV for regeneration. Results from (A) and (B) suggest incomplete sulfation due to the presence of multiple sulfated products.

As can be seen above, use of 0.750mM hexasaccharide compound and 3.25mM PNPS showed no advantage for sulfation. Furthermore, previous lab members had also attempted an AST-IV regeneration system and were unsuccessful as well. Therefore, use of the PAPS regeneration system was abandoned.

Phosphatase as a method of degrading PAP/PAPS

As a last attempt to see if possible product inhibition by PAP could be avoided, a degradation system using phosphatase was proposed. The first step was to see if phosphatase (Sigma-Aldrich) was capable of degrading PAPS. To check for degradation, the reaction was analyzed using HPLC and anion exchange chromatography via polyamine column. The flow was set to 1mL/min using a high salt elution with a 0-100% gradient of KH_2PO_4 over 20 minutes. Absorption was detected via the adenine absorption of the degraded PAP/PAPS with UV-Vis absorbance at 260nm. As can be seen below the degradation was quite successful (Figure 24):

A) PAPS: 500µM

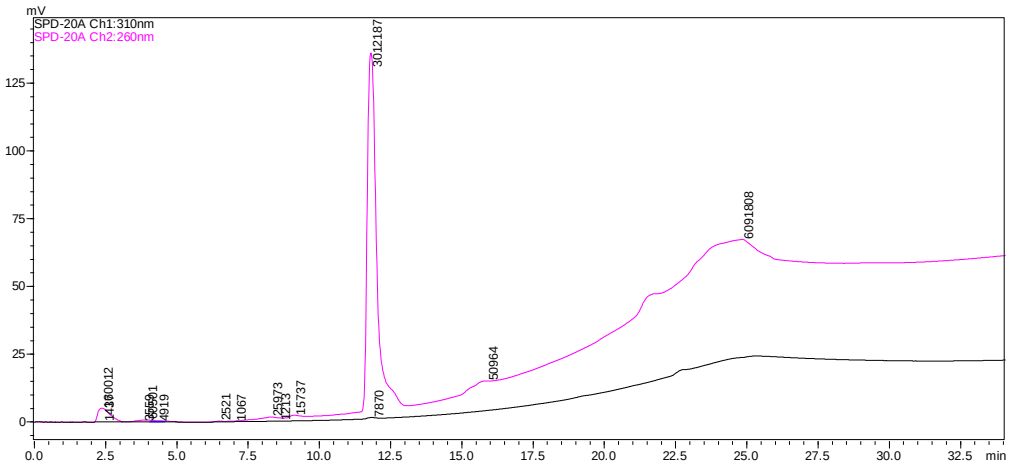

B) PAP 500µM

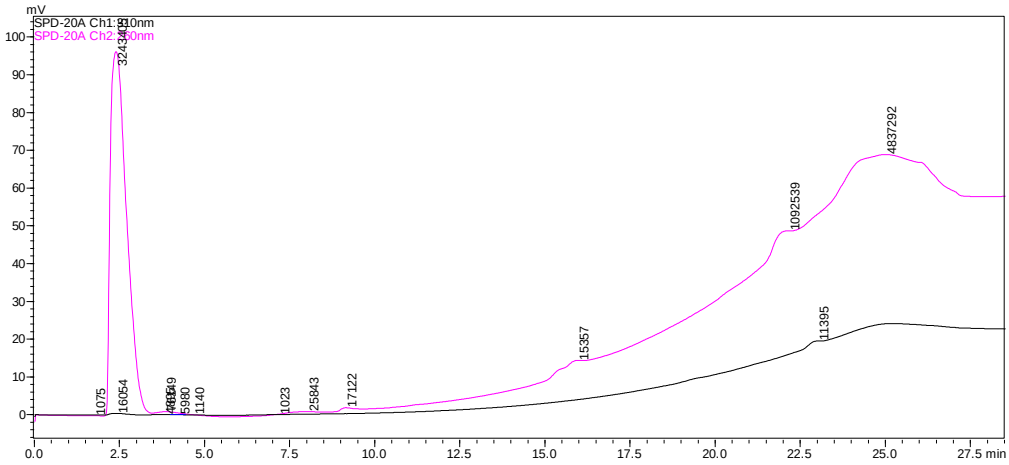

Figure 24: Chromatograms of PAP/PAPS degradation. (A) represents a chromatogram of phosphatase degradation of 500µM PAPS. (B) represents a chromatogram of phosphatase degradation of 500µM PAP. Both show complete degradation. The degradation occurred over the course of one day.

However, there was difficulty in removing the phosphatase enzyme when it was directly added to the reaction, so a dialysis bag was used. As can be seen below it slowed the degradation process, but could still be completed in two days (Figure 25):

A) Phosphatase in Dialysis Bag Day 1

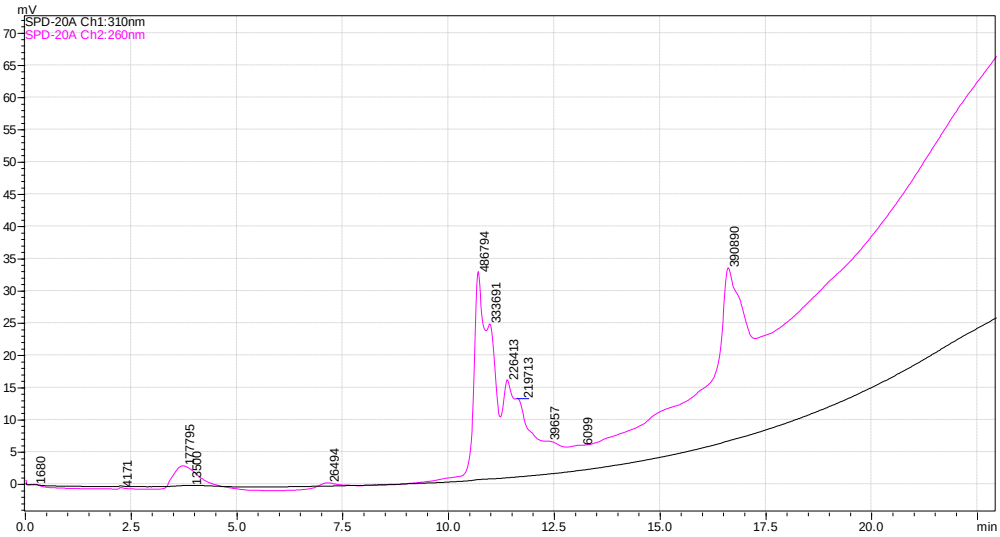

B) Phosphatase in Dialysis Bag Day 2

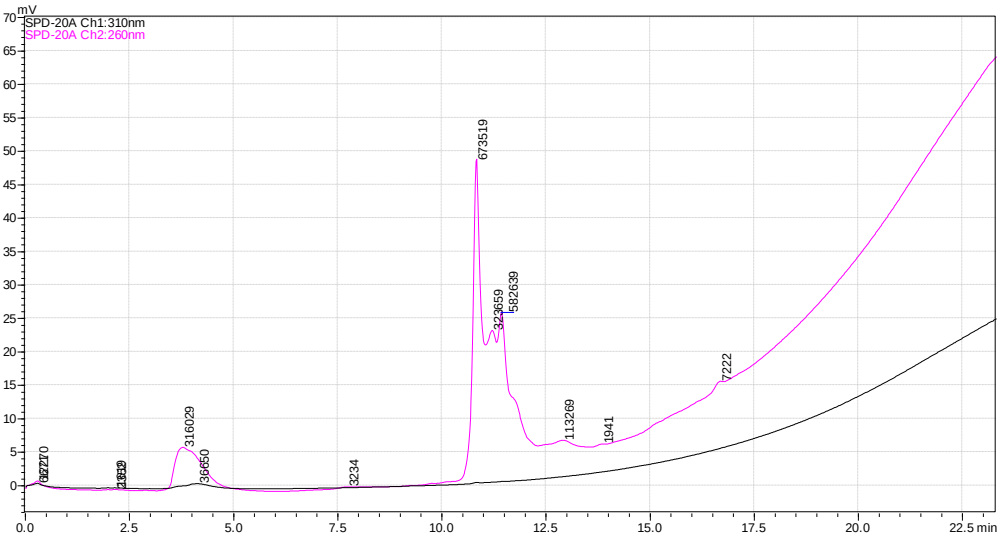

Figure 25: Chromatograms of phosphatase degradation with dialysis bag (A) represents a chromatogram of phosphatase degradation on day 1 and shows incomplete degradation. (B) represents a chromatogram of phosphatase degradation on day 2 and shows complete degradation.

However, we needed to see if this same technique could be used for a sulfation reaction to drive it to completion. Therefore, we started a 6-O sulfation reaction as mentioned previously and added the dialysis bag of phosphatase after 24 hours. We then tried to add more PAPS and 6-OST to drive the sulfation forward. The results of our attempts can be seen below (Figure 26):

A) Dialysis bag with phosphatase degradation and further sulfation

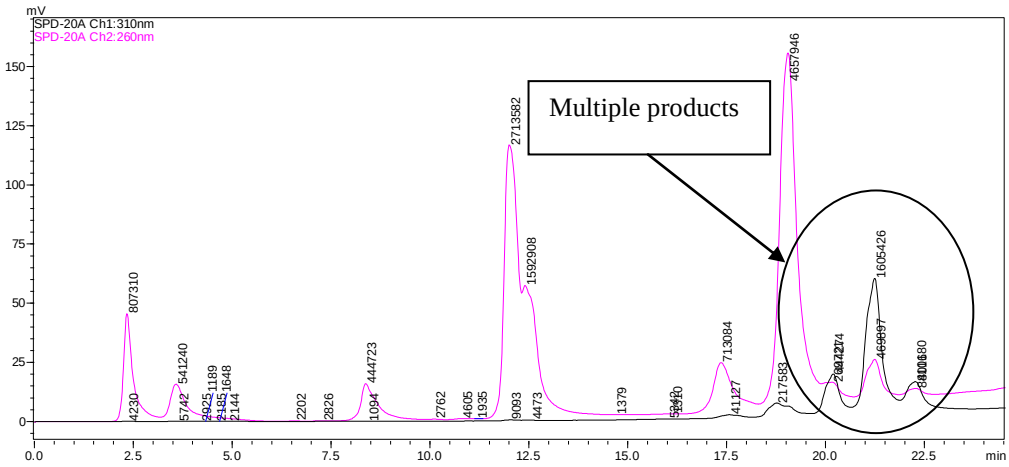

B) No phosphatase degradation

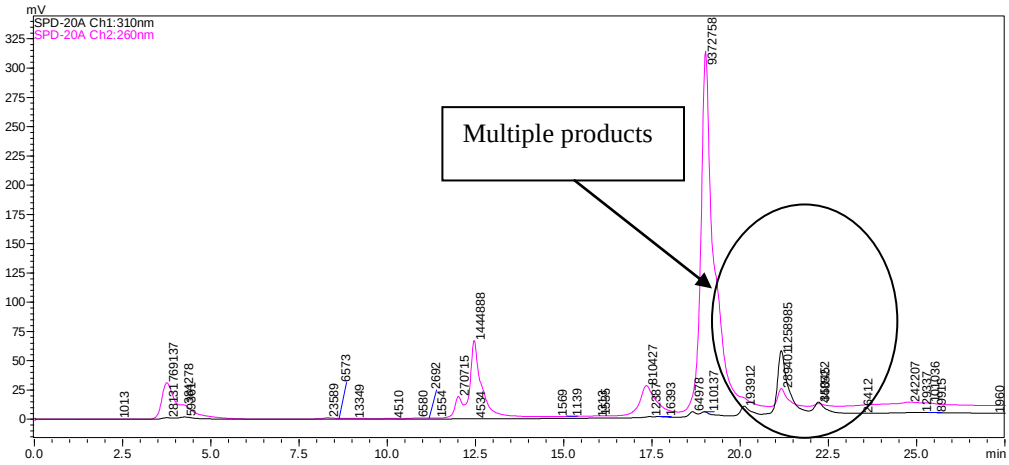

Figure 26: Chromatograms of phosphatase degradation with dialysis bag (A) represents a chromatogram of the second sulfation attempt after PAPS/PAP degradation using a dialysis bag containing phosphatase. (B) represents a chromatogram of the second sulfation attempt with no PAPS/PAP degradation. Results from (A) and (B) suggest incomplete sulfation in both situations, indicating the degradation likely does not have an impact on the results in a manner useful for implementation of PAPS/PAP degradation.

As can be seen from above, the degradation of PAP/PAPS did not change the reaction progression.

Conclusions and Future Directions

As of now, it still remains inconclusive as to what is causing chemoenzymatic sulfations to become difficult as the HS backbone grows. However, we are now aware that the PAPS/PAP degradation and or a regeneration system do not offer an adequate solution for pushing the reaction forward. The next steps could involve better purification techniques and/or expressing enzymes with better activity.

REFERENCES

1. Fu, L.; Suflita, M.; Linhardt, R. J. Bioengineered heparins and heparan sulfates. *Advanced Drug Delivery Reviews*. **2016**, *97*, 237–249.

2. Peterson, S.; Frick, A.; Liu, J. Design of biologically active heparan sulfate and heparin using an enzyme-based approach. *Natural Product Reports*. **2009**, *26*, 610-627.

3. Jackson R. L.; Busch, S. J.; Cardin, A.D. Glycosaminoglycans: molecular properties, protein interactions and role in physiological processes. *Physiological Reviews.* **1991**, *71(2),* 481-539.

4. Salmivirta, M.; Lidholt, K.; Lindahl, U. Heparan sulfate: a piece of information. *The FASEB Journal.* **1996**, *10(11),* 1270-1279.

5. Misra, S.; Hascall, V. C.; Atanelishvili, I.; Rodriguez, R. M.; Markwald, R. R.; Ghatak, S. Utilization Of Glycosaminoglycans/Proteoglycans as Carriers for Targeted Therapy Delivery. *International Journal of Cell Biology*. **2015**, *2015*, 1–25.

6. Hardingham, T. E.; Fosang, A. J. Proteoglycans: many forms and functions. *The FASEB Journal.* **1992,** *6(3),* 861-870.

7. Rabenstein, D. L. Heparin and heparan sulfate: structure and function. *Natural Product Reports*. **2002**, *19*, 312-331.

8. Iozza, R.V. Heparan sulfate proteoglycans: intricate molecules with intriguing functions. *The Journal of Clinical Investigation.* **2001**, *108(2),* 165-167.

9. Lever, R.; Mulloy, B.; Page, C. P. *Handbook of Experimental Pharmacology 207*; Springer: Berlin; New York, 2012.

10. EXT1 gene. Genetics Home Reference, http://ghr.nlm.nih.gov/gene/ext1 (accessed Feb 15, 2016).

11. EXT2 gene. Genetics Home Reference, http://ghr.nlm.nih.gov/gene/ext2 (accessed Feb 15, 2016).

12. Chappell, E. P.; Liu, J. Use of biosynthetic enzymes in heparin and heparan sulfate synthesis. *Bioorganic and Medicinal Chemistry* **2013**, *21*, 4786-4792.

13. Esko, J. D.; Lindahl, U. Molecular diversity of heparan sulfate. *The Journal of Clinical Investigation*. **2001**, *108(2),* 169-173.

14. Hammond, E.; Khurana, A.; Shridhar, V.; Dredge, K. The role of heparanase and sulfatases in the modification of heparan sulfate proteoglycans within the tumor

microenvironment and opportunities for novel cancer therapeutics. *Frontiers in Oncology*. **2014**, *4(195)*, 1-15.

15. Tumova, S.; Woods, A.; Couchman, J. R.; Heparan sulfate proteoglycans on the cell surface: versatile coordinators of cellular functions. *The International Journal of Biochemistry & Cell Biology*. **2000**, *32(3)*, 269–288.

16. Surviladze, Z.; Sterkand, R. T.; Ozbun, M. A. Interaction of human papilloma virus type 16 particles with heparan sulfate and syndecan-1 molecules in the keratinocyte extracellular matrix plays an active role in infection. *Journal of General Virology***. 2015**, *96(8)*, 2232-41.

17. Liu, J.; Thorp, S. C. Cell Surface Heparan Sulfate and Its Roles in Assisting Viral Infections. *Medicinal Research Reviews.* **2002,** *22(1)*, 1-25.

18. 2014 Sexually Transmitted Diseases Surveillance. Centers for Disease Control and Prevention, http://www.cdc.gov/std/stats14/other.htm#herpesc (accessed Feb 16, 2016).

19. Guimond, S. E.; Turnbull, J. E. Fibroblast growth factor receptor signaling is dictated by specific heparan sulfate saccharides. *Current Biology.* **1999**, *9(22)*, 1343-1346.

20. Tarbell, J. M.; Cancel, L. M. The glycocalyx and its significance in human medicine. *Journal of Internal Medicine*. **2016.**

21. Bishop, J. R.; Schuksz, M.; Esko, J. D. Heparan sulfate proteoglycans fine-tune mammalian physiology. *Nature.* **2007**, *446*, 1030-1037.

22. Soares, M. A.; Teixeira, F. C. O. B.; Fontes, M.; Arêas, A. L.; Leal, M. G.; Pavão, M. S. G.; Stelling, M. P. Heparan Sulfate Proteoglycans May Promote Or Inhibit Cancer Progression by Interacting with Integrins and Affecting Cell Migration. *BioMed Research International*. **2015**, *2015*, 1–8.

23. Kumar, A.; Katakam, S.; Urbanowitz, A. K.; Gotte, M. Heparan Sulphate as a Regulator of Leukocyte Recruitment in Inflammation. *Current Protein & Peptide Science.* **2015**, *16(1)*, 77–86.

24. Wang, L.; Fuster, M.; Sriramaroa, P.; Esko. J. D. Endothelial heparan sulfate deficiency impairs L-selectin and chemokine mediated neutrophil trafficking during inflammatory responses. *Nature Immunology.* **2005,** *6(9)*, 902-910.

25. Brummel-Ziedens, K.; Mann, K. G. Molecular Basis of Blood Coagulation. In Hematology Basic Principles and Practice; Hoffman, R., Ed.; Elsevier Saunders: Philadelphia, PA, 2013; pp. 1821–1841.

26. Warkentin, T. E. Heparin-Induced Thrombocytopenia. In Hematology Basic Principles and Practice; Hoffman, R., Ed.; Elsevier Saunders: Philadelphia, PA, 2013; pp. 1913-1924.

27. Greinacher, A. Heparin-Induced Thrombocytopenia. *New England Journal of Medicine*. **2015,** *373(3),* 252-261.

28. Heparin (unfractionated): Drug information. UpToDate, http://www.uptodate.com.libproxy.lib.unc.edu/contents/therapeutic-use-of-unfractionated-heparin-and-low-molecular-weight-heparin?source=search_result (accessed Feb 17, 2016).

29. Hull, R. D.; Garcia, D. A. Therapeutic use of unfractionated heparin and low molecular weight heparin. UpToDate, http://www.uptodate.com/contents/therapeutic-use-of-unfractionated-heparin-and-low-molecular-weight-heparin?source=search_result (accessed Feb 17, 2016).

30. Enoxaparin: Drug Information. UpToDate, http://www.uptodate.com/contents/enoxaparin-drug-information?source=search_result&search=lmwh&selectedTitle=3~150 (accessed Feb 17, 2016).

31. Fondaparinux: Drug Information. UpToDate, http://www.uptodate.com.libproxy.lib.unc.edu/contents/fondaparinux-drug-information?source=see_link#F174020 (accessed Feb 17, 2016).

32. Woody, S. M. Enzymatic Synthesis of UDP-Glucuronic Acid from glucose. Honors Thesis, University Of North Carolina at Chapel Hill, 2015.

33. Chandarajoti, K.; Xu, Y.; Sparkenbaugh, E.; Key, N. S.; Pawlinski, R.; Liu, J. De novo synthesis of a narrow size distribution low molecular weight heparin. *Glycobiology*. **2014**, *24(5)* 476-486.

34. Merli, G. J.; Groce, H. M. Pharmacological and clinical differences between low-molecular-weight-heparins. *P&T*. **2010**, *35(2),* 95-105.

35. Dai, X.; Liu, W.; Zhou, Q.; Cheng, C.; Yang, C.; Wang, S.; Zhang, M.; Tang, P.; Song, H.; Zhang, D.; Qin, Y. Formal Synthesis Of Anticoagulant Drug Fondaparinux Sodium. *The Journal of Organic Chemistry.* **2016**, *81(1)*, 162–184.

36. Petitou, M.; van Boeckel, C. A. A Synthetic Antithrombin III Binding Pentasaccharide Is Now a Drug! What Comes Next? *Angewandte Chemie International Edition.* **2004**, *43(24)*, 3118–3133.

37. Bauer, K. A. Therapeutic use of fondaparinux .UpToDate, http://www.uptodate.com.libproxy.lib.unc.edu/contents/therapeutic-use-of-fondaparinux?source=see_link#H831144 (accessed Feb 18, 2016).

38. Xu, Y.; Masuko, S.; Takieddin, M.; Xu, H.; Liu, R.; Jing, J.; Mousa, S. A.; Linhardt, R. J.; Liu, J. Chemoenzymatic Synthesis of Homogenous Ultralow Molecular Weight Heparins. *Science*. **2011**, *334*, 498-501.

39. Liu, H.; Zhang, Z.; Linhardt, R. J. Lessons learned from the contamination of heparin. *Natural Product Reports.* **2009,** *26(3),* 313-321.

40. Liu, J.; Linhardt, R. J. Chemoenzymatic synthesis of heparan sulfate and heparin. *Natural Product Reports.* **2014,** *31,* 1676-1685.

41. Xu, Y.; Cai, C.; Chandarajoti, K.; Hsieh, P. H.; Li, L.; Pham, T. Q.; Sparkenbaugh, E. M.; Sheng, J.; Key, N. S.; Pawlinski, R.; Harris, E. N.; Linhardt, R. J.; Liu, J. Homogeneous Low-Molecular-Weight Heparins with Reversible Anticoagulant Activity. *Nature Chemical Biology.* **2014**, *10(4),* 248–250.

42. α-D-Glucosamine 1-phosphate. Sigma-Aldrich Co., http://www.sigmaaldrich.com/catalog/product/sigma/g9753?lang=en (accessed Feb 19, 2016).

43. α-D-Glucosamine hydrochloride. Sigma-Aldrich Co., http://www.sigmaaldrich.com/catalog/product/sigma/g4875?lang=en&region=US (accessed Feb 19, 2016).

44. Uridine 5′-diphosphoglucuronic acid trisodium salt Sigma-Aldrich Co., http://www.sigmaaldrich.com/catalog/product/sigma/u6751?lang=en&region=US (accessed Feb 19, 2016).

45. D-(+)-Glucose. Sigma-Aldrich Co., http://www.sigmaaldrich.com/catalog/product/sigma/g8270?lang=en&region=US (accessed Feb 19, 2016).

46. Liu, R.; Xu, Y.; Chen, M.; Weïwer, M.; Zhou, X.; Bridges, A. S.; DeAngelis, P. L.; Zhang, Q.; Linhardt, R. J.; Liu J. Chemoenzymatic Design of Heparan Sulfate Oligosaccharides. *The Journal of Biological Chemistry.* 2**010**, *285(44),* 34240-34249.

47. Zhao, G.; Guan, Q.; Cai, L.; Wang, P. G. Enzymatic route to preparative-scale synthesis of UDP-GlcNAc/GalNAc, their analogues and GDP-fucose. *Nature Protocols*. **2010,** *5(4),* 636-646.

48. Egger, S.; Chaikuad, A.; Kavanagh, K. L.; Oppermann, U.; Nidetzky, B. Structure and Mechanism of Human UDP-Glucose 6-Dehydrogenase. *The Journal of Biological Chemistry.* **2011**, *286(27),* 23877–23887.

49. Toone, E. J.; Simon, E. S.; Whitesides, G. M. Enzymatic synthesis of uridine 5' diphosphoglucuronic acid on a gram scale. *The Journal of Organic Chemistry*. **1991,** *56 (19),* 5603-5606.

50. Simon, E. S.; Grabowski, S.; Whitesides, G. M. Convenient Syntheses of cytidine 5'-triphosphate, guanosine 5'-triphosphate and uridine 5'-triphosphate and their use in the preparation of UDP-glucose, UDP-glucuronic Acid and GDP-mannose. *The Journal of Organic Chemistry*. **1990,** *55(6),* 1834-1841.

51. Wong, C. H.; Haynie, S. L.; Whitesides, G. M. Enzyme-catalyzed synthesis of N-acetyllactosamine with in situ regeneration of uridine 5'-diphosphate glucose and uridine 5'-diphosphate galactose. *The Journal of Organic Chemistry*. **1982,** *42(27),* 5416-5418.

52. Heidlas, J. E.; Williams, K. W.; Whitesides, G. M. Nucleoside phosphate sugars: syntheses on practical scales for use as reagents in the enzymatic preparation of oligosaccharides and glycoconjugates. *Accounts of Chemical Research*. **1992,** *25(7),* 307-314.

53. Wong, C-H.; Haynie, S. L.; Whitesides, G. M. Preparation of a mixture of nucleoside triphosphates from yeast RNA: use in enzymatic synthesis requiring nucleoside triphosphate regeneration and conversion to nucleoside diphosphate sugars. *Journal of the American Chemical Society*. **1983,** *105(1),* 115-117.

54. Hirschbein, B. L.; Mazenod, F. P.; Whitesides, G. M. Synthesis of phosphoenolpyruvate and its use in ATP cofactor regeneration. *The Journal of Organic Chemistry*. **1982,** *47(19),* 3765-3766.

55. Heidlas, J. E.; Lees, W. J.; Pale, P.; Whitesides, G. M. Gram scale synthesis of uridine 5'-diphospho-N-acetylglucoasmine: comparison of enzymatic and chemical routes. *The Journal of Organic Chemistry*. **1992,** *57(1),* 146-151.

56. Sommer, B. J.; Barycki, J. J.; Simpson, M. A. Characterization of human UDP-glucose Dehydrogenase: Cys-276 is required for the second of two successive oxidations. *The Journal of Biological Chemistry.* **2004,** *279(22),* 23590-23596.

57. Stewart, D. C.; Copeland, L. Uridine 5'-diphosphate-glucose dehydrogenase from soybean nodules. *Plant Physiology.* **1998,** *116(1),* 349-355.

58. Turner, W.; Botha, F. C. Purification and kinetic properties of UDP-glucose dehydrogenase from sugarcane. *Archives of Biochemistry and Biophysics.* **2002,** *407(2),* 209-216.

59. Fromm, H. J.; Zewe, V. Kinetic Studies of the Brain Hexokinase Reaction. *The Journal of Biological Chemistry*. **1962**, *237(5),* 1661-1667.

60. Fromm, H. J.; Zewe, V. Kinetic Studies of Yeast Hexokinase. *The Journal of Biological Chemistry.* **1962**, *237(10)*, 3027-3032.

61. Peláez, R.; Fernández-García, P.; Herrero, P.; Moreno F. Nuclear Import of Yeast Hexokinase 2 Protein Requires α/β-Importin-dependent Pathway. *The Journal of Biological Chemistry.* **2012,** *287(5)*, 3518-3529.

62. Renz, A., Merlo, L. & Stitt, M. Partial purification from potato tubers of three fructokinases and three hexokinases which show differing organ and developmental specificity. *Planta*. **1993,** *190(2)*, 156-165.

63. Barstow, D. A.; Black, G. W.; Sharman, A. F.; Scawen, M. F.; Atkinson, T.; Li, S. S.; Chia, W. N.; Clarke, A. R.; Holbrook, J. J. Expression of the copy DNA for human A4 and B4 Lactate dehydrogenases in Escherichia Coli. *Biochimica et Biophysica Acta*. **1990,** *1087(1)*, 73-79.

64. Hewitt, C. O.; Eszes, C. M.; Sessions, R. B.; Moreton, K. M.; Daffron, T. R.; Takei K.; Dempset, C. E.; Clarke, A. R.; Holbrook, J. J. A general method for relieving substrate inhibition in lactate dehydrogenases. *Protein Engineering* **1999,** *12(6)* 491-496.

65. Nakano, K.; Omura, Y.; Tagaya, M.; Fukui, T. UDP-Glucose Pyrophosphorylase from Potato Tuber: Purification and Characterization. *The Journal of Biochemistry*. **1989,** *106(3)*, 528-532.

66. Martz, F.; Wilczynska, M.; Kleczkowski, L. A. Oligomerization status, with the monomer as active species, defines catalytic efficiency of UDP-glucose pyrophosphorylase. *Biochemical Journal*. **2002**, *367(1)*, 295-300.

67. Uridine 5′-diphosphoglucose disodium salt hydrate from *Saccharomyces cerevisiae.* Sigma-Aldrich Co., http://www.sigmaaldrich.com/catalog/product/sigma/u4625?lang=en&region=US. (accessed Feb. 22, 2016).